



**HAL**  
open science

# Use of computational fluid dynamic tools to model the coupling of plant canopy activity and climate in greenhouses and closed plant growth systems: A review

Hicham Fatnassi, Pierre Emmanuel Bournet, Thierry Boulard, Jean-Claude Roy, Francisco Domingo Molina Aiz, Rashyd Zaaboul

## ► To cite this version:

Hicham Fatnassi, Pierre Emmanuel Bournet, Thierry Boulard, Jean-Claude Roy, Francisco Domingo Molina Aiz, et al.. Use of computational fluid dynamic tools to model the coupling of plant canopy activity and climate in greenhouses and closed plant growth systems: A review. *Biosystems Engineering*, 2023, 230, pp.388 - 408. 10.1016/j.biosystemseng.2023.04.016 . hal-04224324

**HAL Id: hal-04224324**

**<https://hal.science/hal-04224324v1>**

Submitted on 2 Oct 2023

**HAL** is a multi-disciplinary open access archive for the deposit and dissemination of scientific research documents, whether they are published or not. The documents may come from teaching and research institutions in France or abroad, or from public or private research centers.

L'archive ouverte pluridisciplinaire **HAL**, est destinée au dépôt et à la diffusion de documents scientifiques de niveau recherche, publiés ou non, émanant des établissements d'enseignement et de recherche français ou étrangers, des laboratoires publics ou privés.

# Biosystems Engineering

## Use of Computational Fluid Dynamic tools to model the coupling of plant canopy activity and climate in greenhouses and closed plant growth systems: a review.

--Manuscript Draft--

<b>Manuscript Number:</b>	YBENG-D-22-01328R2
<b>Article Type:</b>	Review Article
<b>Keywords:</b>	Greenhouse; Crop Model; plant; Transpiration; photosynthesis; cfd; Porous Medium; User Defined Function UDF
<b>Corresponding Author:</b>	Hicham Fatnassi International Center for Biosaline Agriculture UNITED ARAB EMIRATES
<b>First Author:</b>	Hicham Fatnassi
<b>Order of Authors:</b>	Hicham Fatnassi Pierre Emmanuel Bournet Thierry Boulard Jean Claude Roy Francisco D. Molina-Aiz Rashyd Zaaboul
<b>Manuscript Region of Origin:</b>	Middle East
<b>Abstract:</b>	<p>Since the 1990s, CFD has allowed significant progress in the distributed climate and crop modeling in greenhouses. The quality of CFD modeling chiefly relies on its capacity to depict the dynamic interaction of the crop with airflow and the subsequent heat and mass exchanges. CFD approach combines different scales of modeling, i.e., the greenhouse and its environment with the crop canopy, with an accuracy of a few cubic centimeters. This approach accounts for the coupling of air transfers within the crop assimilated to the solid matrix of a porous medium exchanging momentum, heat, and mass with air. The sink and source terms for momentum, sensible and latent heat fluxes, and other mass exchanges are assigned to each cell of the porous medium. The local air velocity, temperature, humidity, and radiation can be calculated by solving the conservation equations together with the radiative transfer equation. The crop canopy's CO<sub>2</sub> and evapotranspiration distributions are deduced from the locally distributed climate.</p> <p>In this paper, the coupling of the plant activity with its local microclimate using the CFD modeling approach is described in detail. Its implementation through a User Defined Function (UDF) coupling the crop submodel to the main CFD solver is also provided. The primary studies related to the CFD modeling of crops inside greenhouses are reviewed concerning various interactions such as loss of momentum, transpiration, photosynthesis, and the characteristics of the field experiments used for validations. From this analysis, future trends of CFD developments applied to crop activity are also presented.</p>
<b>Suggested Reviewers:</b>	In-Bok Lee, Professor Seoul National University iblee@snu.ac.kr  Murat Kacira, Professor The University of Arizona mkacira@email.arizona.edu
<b>Opposed Reviewers:</b>	
<b>Response to Reviewers:</b>	

## CONFLICT OF INTEREST

**Manuscript title:** Use of Computational Fluid Dynamic tools to model the coupling of plant canopy activity and climate in greenhouses and closed plant growth systems: a review.

The authors whose names are listed immediately below certify that they have NO affiliations with or involvement in any organization or entity with any financial interest (such as honoraria; educational grants; participation in speakers' bureaus; membership, employment, consultancies, stock ownership, or other equity interest; and expert testimony or patent-licensing arrangements), or non-financial interest (such as personal or professional relationships, affiliations, knowledge or beliefs) in the subject matter or materials discussed in this manuscript.

**Author names:**

Hicham Fatnassi

Pierre Emmanuel Bournet

Thierry Boulard

Jean Claude Roy

Francisco D. Molina-Aiz

Rashyd Zaaboul<sup>1,6</sup>

- Mechanical and heat and mass transfers at crop level in CFD modelling
- Radiative transfers within the crop rows in CFD modelling
- Photosynthetic activity, leaf temperature and crop transpiration in CFD modelling
- Simulation of shortwave radiation inside the crop
- Simulation of the distribution of CO<sub>2</sub> concentration in the greenhouse

1 **Use of Computational Fluid Dynamic tools to model the coupling of plant**  
2 **canopy activity and climate in greenhouses and closed plant growth**  
3 **systems: a review.**

4 **Hicham Fatnassi<sup>1,2\*</sup>, Pierre Emmanuel Bournet<sup>3</sup>, Thierry Boulard<sup>4</sup>, Jean Claude Roy<sup>5</sup>,**  
5 **Francisco D. Molina-Aiz<sup>6</sup>, Rashyd Zaaboul<sup>1,6</sup>**

6 <sup>1</sup> International Center for Biosaline Agriculture, ICBA, Dubai, P.O. Box 14660, United Arab Emirates

7 <sup>2</sup> INRA, Univ. Nice Sophia Antipolis, CNRS, UMR 1355-7254 Institut Sophia Agrobiotech, 06900 Sophia Antipolis,  
8 France

9 <sup>3</sup> a, SFR 4207 QuaSaV, 49000, Angers, France

10 <sup>4</sup> 33, Avenue Saint Laurent, 06520, Magagnosc, France.

11 <sup>5</sup> FEMTO-ST, Franche-Comté University, Belfort, France.

12 <sup>6</sup> Departamento de Ingeniería Rural, Universidad de Almería, Escuela Politécnica Superior, Ctra. Sacramento, 04120  
13 Almería, Spain

14

15 Corresponding author e-mail: [h.fatnassi@biosaline.org.ae](mailto:h.fatnassi@biosaline.org.ae)

16

17 **Abstract**

18 Since the 1990s, Computational Fluid Dynamics (CFD) has allowed significant  
19 progress in the distributed climate and crop modelling in greenhouses. The quality of CFD  
20 modelling chiefly relies on its capacity to depict the dynamic interaction of the crop with  
21 airflow and the subsequent heat and mass exchanges. CFD approach combines different  
22 scales of modelling, i.e., the greenhouse and its environment with the crop canopy, with an  
23 accuracy of a few cubic centimetres corresponding to the volume of one mesh cell in the  
24 greenhouse. This modelling approach accounts for the coupling of air transfers within the  
25 crop simulated to the solid matrix of a porous medium exchanging momentum, heat, and  
26 mass with air. The sink and source terms for momentum, sensible and latent heat fluxes,  
27 and other mass exchanges are assigned to each cell of the porous medium (i.e., canopy).

28 The local air velocity, temperature, humidity, and radiation distributions can then be  
29 calculated by solving the conservation equations together with the radiative transfer  
30 equation. The crop canopy's CO<sub>2</sub> distributions and other plant activity parameters (such as  
31 evapotranspiration or photosynthesis) are deduced from the locally distributed climate. In  
32 this paper, the coupling of the plant activity with its local microclimate using the CFD  
33 modelling approach is described in detail. Its implementation through a User Defined  
34 Function (UDF) coupling the crop submodel to the main CFD solver is also provided. The  
35 primary studies related to the CFD modelling of crops inside greenhouses are reviewed  
36 concerning various interactions such as loss of momentum, transpiration, photosynthesis,  
37 and the characteristics of the field experiments used for validations. From this analysis,  
38 future trends of CFD developments applied to crop activity are also presented.

39

40 **Keywords:** Greenhouse, Crop Model, Plant, Transpiration, Photosynthesis, CFD, Porous  
41 Medium, User Defined Function UDF

42

43

## 44 **Nomenclature**

45	$a_1$	Empirically determined parameter
46	$a_2$	Empirically determined parameter
47	$a_3$	Empirically determined parameter
48	$b_1$	Empirically determined parameter
49	$b_2$	Empirically determined parameter
50	$b_3$	Empirically determined parameter
51	$C$	Sensible heat flux density, in $\text{W m}^{-3}$
52	$C_a$	Concentration of $\text{CO}_2$
53	$C_D$	Drag coefficient
54	$C_F$	Non-linear momentum loss coefficient
55	$C_p$	Specific heat at constant pressure, in $\text{J kg}^{-1} \text{K}^{-1}$
56	$d$	Characteristic dimension of the leaves, in m
57	$dV$	Volume element, in $\text{m}^3$
58	$E$	Evaporated water flux, in $\text{kg m}^{-3} \text{s}^{-1}$
59	$Gr$	Grashof number
60	$h_s$	Heat exchange coefficient, in $\text{W m}^{-2} \text{K}^{-1}$
61	$H$	Average height of the crop row, in m
62	$I$	PAR incident radiative flux, in $\text{W m}^{-2}$
63	$K$	Permeability of the porous medium, in $\text{m}^2$
64	$K_C$	Radiation extinction coefficient
65	$L$	Length of the crop row, in m
66	$l$	Width of the crop row, in m
67	$LAD$	Leaf area density, in $\text{m}^2 \text{m}^{-3}$
68	$LAI$	Leaf area index, in $\text{m}^2 \text{m}^{-2}$
69	$L_v$	Heat of vaporisation of water, in $\text{J kg}^{-1}$
70	$Nu$	Nusselt number
71	$P_r$	Photosynthesis flux, in $\text{kg}_{\text{CO}_2} \text{m}^{-3} \text{s}^{-1}$
72	$Pr_t$	Prandtl number
73	$q_l$	Latent heat flux density, in $\text{W m}^{-3}$

74	$q_s$	Convective sensible heat flux density, in $W m^{-3}$
75	$R_{abs}$	Net radiation intercepted by plant leaves, in $W m^{-3}$
76	$Rg_0$	Global radiation intercepted at the top of the crop cover, in $W m^{-2}$
77	$Rg(z)$	Global radiation along the optical path of the sun at a distance $z$ from the top of the canopy,
78		in $W m^{-2}$
79	$r_a$	Aerodynamic resistance, in $s m^{-1}$ .
80	Re	Reynolds number
81	$r_s$	Stomatal resistance, in $s m^{-1}$
82	$r_t$	Total resistance, in $s m^{-1}$
83	$S_{CO_2}$	Net photosynthesis consumption flux, in $kg_{CO_2} m^{-3} s^{-1}$
84	$S_0$	Source term
85	$T_a$	Air temperature, in K
86	$T_l$	Leaf temperature, in K
87	$T_{max}$	Empirically determined parameter, in K
88	U	Component of the velocity vector according to X-axis, in $m s^{-1}$
89	v	Air speed within the crop cover, in $m s^{-1}$
90	V	Component of the velocity vector according to Y-axis, in $m s^{-1}$
91	$VPD_a$	Air-air vapor pressure deficit, in Pa
92	$VPD_0$	Empirically determined parameter, in Pa
93	W	Component of the velocity vector according to Z-axis, in $m s^{-1}$
94	$w_a$	Absolute humidity of the surrounding air, in $kg kg^{-1}$
95	$w_l$	Absolute saturating humidity at the leaf level, in $kg kg^{-1}$
96	z	Distance from the top of the canopy, in m
97	$\Phi$	Concentration of the transported quantity,
98	$\mu$	Dynamic viscosity of air, in $kg m^{-1} s^{-1}$
99	$\Gamma$	Diffusion coefficient, in $kg m^{-1} s^{-1}$
100	$\gamma$	Psychrometric constant, in $Pa K^{-1}$
101	$\Delta$	Slope of the saturated water vapor pressure curve, in $Pa K^{-1}$
102	$\tau$	Leaf conductance, in $m s^{-1}$
103	$\rho$	Air density, in $kg m^{-3}$



104  $\alpha$       Photosynthesis efficiency, in  $\text{kg}_{\text{CO}_2} \text{J}^{-1}$

105  $\lambda_a$       Air conductivity, in  $\text{W m}^{-1} \text{K}^{-1}$

106 **Subscripts**

107  $a$       refers to air

108  $C$       refers to  $\text{CO}_2$

109  $l$       refers to leaf

110  $w$       refers to  $\text{H}_2\text{O}$

111 **Abbreviation**

112 CFD      Computational Fluid Dynamics

113 DO      Discrete ordinates model

114 LAD      Leaf area density

115 LAI      Leaf area index

116 LWD      Leaf Wet Duration

117 RTE      Radiative transfer equation

118 UDF      User-Defined Function

119

## 120 **1. Introduction**

121 Computational Fluid Dynamics is a branch of fluid mechanics that uses numerical analysis  
122 and data structures to solve problems that involve fluid flows. It allows simulating the  
123 distribution of fluid flow variables inside a calculation domain. Considering the words  
124 “Computational Fluid Dynamics”, on the Scopus<sup>TM</sup> database it was found that more than  
125 90 000 CFD papers were published during the 1974 – 2021 period reaching around 9000  
126 papers in 2021. Engineering represented more than 30% of CFD publications, followed by  
127 physics and astrophysics, chemical engineering, energy, mathematics, material science,  
128 computer sciences and environmental sciences.

129 The application of CFD in agriculture area has grown significantly since the end of the 90s  
130 (Norton et al., 2007). The first CFD studies in greenhouses were devoted to ventilation  
131 issues and design optimisation without considering the activity of the crop (Okushima et  
132 al., 1989; Mistriotis et al., 1997 a, b and c). Recent and important progress was observed in  
133 the modelling of the greenhouse distributed climate and particularly the climate at crop  
134 level, by including the effect of the dynamic action of the crop on the flow and the  
135 subsequent heat and mass transfers (Haxaire,1999; Boulard and Wang, 2002; Fatnassi et  
136 al., 2003, 2006, 2015; Majdoubi et al., 2009; Kichah et al., 2012; Tamimi et al., 2013;  
137 Majdoubi et al., 2016; Boulard et al., 2017; Tadj et al., 2017; Bouhoun Ali et al., 2018;  
138 Bouhoun Ali et al., 2019; Baxevanou et al., 2020; Ben Amara et al., 2021; Cheng et al.,  
139 2021; Liu et al., 2021; An et al., 2022).

### 140 **1.1. Dynamic, heat and mass transfers at crop level**

141 Haxaire (1999) was, to our knowledge, the first to integrate the drag and transpiration  
142 effects of plant canopies in the airflow inside the greenhouses by customising a CFD  
143 commercial software CFD2000®, (CFD2000, 1997) by means of source terms. He

144 previously conducted wind tunnel tests to determine the relationship between the crop leaf  
145 area index and the pressure drop produced for different air velocities, calculating the value  
146 of the drag coefficient of a tomato plant canopy. The concept of simulating crop rows inside  
147 a greenhouse using a "porous medium" was first introduced by Haxaire (1999). Due to the  
148 complex geometry of real crop rows in a greenhouse, which demands a powerful computer  
149 and is time-consuming, he opted to model crop rows as parallelepiped-shaped porous  
150 media. This approach consists of a solid matrix (representing the plants) with  
151 interconnected pores (representing air). Boulard and Wang (2002) carried out CFD  
152 simulations of a lettuce crop transpiration inside a plastic tunnel including both global solar  
153 radiation transfers and crop heat exchanges while Roy and Boulard (2003) predicted natural  
154 ventilation and climate in a tunnel-type greenhouse using the same crop submodel adapted  
155 to tomato and considering the crop as a porous medium. For tomato plants, they simulated  
156 each mesh of the crop subdomain to volumetric heat and water vapor sources. The radiative  
157 flux was partitioned into convective sensible and latent heat fluxes (depending on the  
158 stomatal and aerodynamic resistances) inside a virtual solid matrix of the porous medium.  
159 This matrix representing the crop was characterised by its leaf temperature and its drag  
160 coefficient (Haxaire, 1999; Boulard and Wang, 2002; Boulard et al., 2002).

161 Fatnassi et al. (2003) adapted the CFD code to simulate the sensible and latent heat  
162 exchanges of tomato plants in a large-scale Canarian greenhouse, and later in a multispan  
163 plastic greenhouse equipped with insect-proof screens (Fatnassi et al. 2006). Similarly, Liu  
164 et al. (2021) and An et al. (2022) customised the CFD code to model cucumber and tomato  
165 transpiration and condensation on leaves in Chinese Solar Greenhouses (CSG), using a  
166 similar approach.

167

168 **1.2. Photosynthetic activity**

169 CFD modelling also focused on photosynthesis, which is another important parameter of  
170 plant activity. Reichrath et al. (2001) developed a CFD model of a large commercial Venlo-  
171 type glasshouse that included the crop as a carbon dioxide sink, following the formulation  
172 proposed by Acock et al. (1978). In their studies, the uptake of CO<sub>2</sub> for photosynthetic  
173 activity was assumed to be proportional to the CO<sub>2</sub> concentration and leaf area index (Hand,  
174 1973).

175 There was apparently no further development on this topic until Roy et al. (2014) and  
176 Boulard et al. (2017) implemented a CFD model to simulate photosynthesis. They  
177 simulated the transpiration rate in a closed greenhouse together with the leaf gross  
178 photosynthesis flux as a function of the CO<sub>2</sub> concentration and incident photosynthetically  
179 active radiation from the model proposed by Thornley (1976) and the calculated  
180 transpiration and photosynthesis rates were then compared with experimental results based  
181 on direct measurements.

182 More recently Molina et al. (2017) developed a CFD model to simulate photosynthesis in  
183 an Almeria-type greenhouse by incorporating the Acock's model.

184 **1.3. Validation of the greenhouse-crop model**

185 The combination of numerical modelling and climate characterisation studies has allowed  
186 the validation of these numerical greenhouse-crop models for air temperature, humidity, air  
187 velocity, and ventilation rate in multispans plastic-houses (Haxaire, 1999; Fatnassi et al.,  
188 2006), large greenhouse-tunnels (Boulard and Wang, 2002; Nebbali et al., 2012) large scale  
189 Canarian type plastic-houses (Fatnassi et al., 2003; Majdoubi et al., 2009), single span  
190 greenhouses (Bartzanas et al., 2002), Venlo-type closed greenhouse equipped with air  
191 conditioners (Boulard et al., 2017) and Chinese Solar Greenhouses (CSG) (Wang et al.,

192 2013; Zhang et al., 2016; Tong et al., 2018; Jiao et al., 2020; Liu et al., 2021; Xiaoyang et  
193 al., 2021; An et al., 2022). The realism of the results and the good fit which were generally  
194 observed between measured and simulated values of the climate fields in all these studies  
195 give confidence in the use of these coupled microclimate-crop numerical models .

#### 196 **1.4. Improving the canopy representation in CFD crop models**

197 As previously reviewed, the canopy considered as a “porous medium” is one of the main  
198 phenomenological approaches of the physical transfers within the crop cover, however, it  
199 is not the only one and plant-CFD modelling can be based on approaches which try to  
200 consider the exact form of leaves and plants, even of stomata. Thus, a numerical model  
201 based on the energy balance has been combined with the Fluent CFD code for computing  
202 temperature and humidity at leaf surface for single bean leaves at low light levels (Roy et  
203 al., 2008). Defraeye et al. (2014) developed an innovative three-dimensional CFD cross-  
204 scale modelling approach to investigate convective mass transport from leaves. Notably,  
205 they bridged the gap between stomatal and leaf scale by including all these scales in the  
206 same computational model, which implies explicitly modelling individual stomata. More  
207 recently, Yu et al. (2022) numerically investigated the effects of natural light and  
208 ventilation on a 3D tomato body climate distribution in a Venlo greenhouse with CFD. The  
209 3D tomato model built based on SolidWorks allows to set up with realism the radiative and  
210 convective (sensible) transfers, however plant transpiration was not considered in the  
211 model.

#### 212 **1.5. Scope of the present paper**

213 Based on this literature review, previous studies reveal that the equivalent porous medium  
214 approach can cover successfully all the bio-physical transfers implied in the plant-climate

215 interactions. For that reason, this paper focuses on CFD crop submodels using the porous  
216 medium concept and shows how to implement heat, and mass exchanges in such models.  
217 As the studied numerical model is composed of two sub models i.e., physical and  
218 ecophysiological, that form two loops exchanging data, an overall description of the CFD  
219 model will be first presented before the different steps of including the various heat and  
220 mass exchanges between the plant and its environment are listed. A detailed description of  
221 how to implement crop interactions with local environment in the CFD modelling follows,  
222 as well as the instructions to calculate the corresponding fluxes in the computer language,  
223 are given. Finally, the main results obtained from CFD simulations using a crop submodel  
224 are summarised and discussed.

## 225 **2. Description of the CFD numerical model**

### 226 **2.1. Fundamentals of CFD applied to greenhouses**

227 The CFD modelling approach of the greenhouse system is based on the combination of  
228 fluxes in different elements of a 3D domain i.e., the greenhouse and its immediate  
229 environment, together with the equipment and crop inside the greenhouse itself, the crop  
230 being simulated to a porous medium that exchanges heat and water vapor with the ambient  
231 environment (Fatnassi et al., 2003; Fatnassi et al., 2006). This model has been adapted from  
232 Haxaire (1999) and Boulard & Wang (2002) to evaluate the airflow, temperature, and  
233 humidity patterns in a real size greenhouse.

234 CFD is based on the solution of a set of equations for the mass, momentum, and energy  
235 conservation:

$$236 \quad \frac{\partial(U\Phi)}{\partial x} + \frac{\partial(V\Phi)}{\partial y} + \frac{\partial(W\Phi)}{\partial z} = \Gamma \cdot \nabla^2 \Phi + S_\Phi \quad (1)$$

237 where  $\Phi$  represents the concentration of the transported quantity, namely the scalar mass  
238 fraction, the three-dimensional velocity components (Navier-Stokes) and the temperature;  
239  $U$ ,  $V$  and  $W$  are the components of the velocity vector;  $\Gamma$  is the diffusion coefficient; and  
240  $S_{\phi}$  is the source term.

241 Advanced computational fluid mechanics software (such as CFD2000 ©, (CFD2000, 1997)  
242 or Ansys Fluent ©, (Ansys, 2010)) was used by most authors in the last two decades to  
243 solve these highly non-linear equations using a spatial finite volume discretisation. Two  
244 main discretisation methods are used in naturally ventilated greenhouses, one is based on  
245 the Finite Element Method (FEM) and the second one on the Finite Volume Method  
246 (FVM). FVM software (mainly ANSYS/FLUENT v 6.3.) is the most frequently used.  
247 Molina et al. (2010) conducted a specific study to compare the respective advantages and  
248 constraints of both methods. The FVM method involves discretising the fluid domain into  
249 a set of control volumes, and approximating the fluxes of mass, momentum, and energy  
250 across the boundaries of these volumes. This discretisation method is widely used in CFD  
251 simulations due to its ability to handle complex geometries and unstructured meshes while  
252 conserving mass, momentum, and energy, which are crucial for accurate simulations.

253 The 3D conservation equations (Eq. 1) for mass, momentum, and energy are solved  
254 together and coupled with the radiative transfer equation (RTE) in transparent (air) media  
255 using mostly the discrete ordinates (DO) model which performs a space discretisation in  
256 several solid angles (Nebbali et al., 2012) and makes it possible to cope with the integral  
257 term of the RTE. In greenhouse CFD studies, the global radiation distribution inside the  
258 canopy was initially assessed from the application of the Beer's law, for a vertical incident  
259 radiation or considering the sun's path in the sky (Nebbali et al., 2012). An extinction

260 coefficient within the canopy was also imposed. This simplified approach made it however  
261 difficult to correctly solve the energy balance inside the canopy.

262 But recently, thanks to an adequate parameterisation setting (Boulard et al., 2017) the  
263 radiative transfer equation (RTE) in semi-transparent (crop rows) media was solved along  
264 with the transfers in transparent (air) media using the discrete ordinates (DO) model. It  
265 means that the coupling between radiative and convective transfer was automatically  
266 performed by the CFD software for the solid and fluid interfaces and the canopy is  
267 considered as a semi-transparent medium interfering also with radiations. The net short  
268 waves radiative balance for each mesh of the crop cover is provided by the software and  
269 added to the net long wave radiative balance. This global net radiative flux is then  
270 considered as the source term of the energy balance equation that performs the computation  
271 of sensible and latent heat exchanges between each cell of the canopy and air.

## 272 **2.2. Dynamic effect of the canopy on the airflow**

### 273 **2.2.1. Porous medium approach**

274 As describing the geometry of the real plants inside the greenhouse remains quite  
275 complicated, requires a powerful computer, and is time-consuming, we consider plant rows  
276 as a porous medium in the shape of parallelepipeds consisting of a solid matrix (plants),  
277 crossed by a network of interconnected pores (air). It is also assumed that the solid matrix  
278 is rigid (or that it undergoes negligible deformations).

279 In the canopy, the size and distribution of the pores, simulated to the voids between the  
280 leaves and the branches, are irregular. Nevertheless, as noted above, providing a detailed  
281 description of the plants would be quite difficult, thus assimilating the canopy to a porous  
282 medium appears to be the best compromise to consider the influence of plants on the



283 airflow. Moreover, most CFD software consider the porous medium approach in a standard  
284 way with respect to flow exchanges (Ansys-Fluent, 2010).

### 285 2.2.2. Darcy-Forchheimer model

286 While the traditional porous media model proposed by Darcy and completed by  
287 Forchheimer (Kaviany, 1995) was initially developed to describe flows in porous media of  
288 high density and low permeability, it can also be used to describe flow in crop rows, which  
289 are high-permeability media (Bruse, 1995; Green, 1992).

290 Using Ansys Fluent Software facilities, crop rows are simplified and simulated to  
291 parallelepipedal blocks of homogeneous porous medium (Figure 1).

292 The sink of momentum due to the drag effect of the crop is symbolised by the source  
293 term  $S_\phi$  in Eq. (1) and expressed by the unit volume of the cover by the commonly used  
294 formula (Thom, 1971; Wilson, 1985):

$$295 \quad S_\phi = -LADC_D v^2 \quad (2)$$

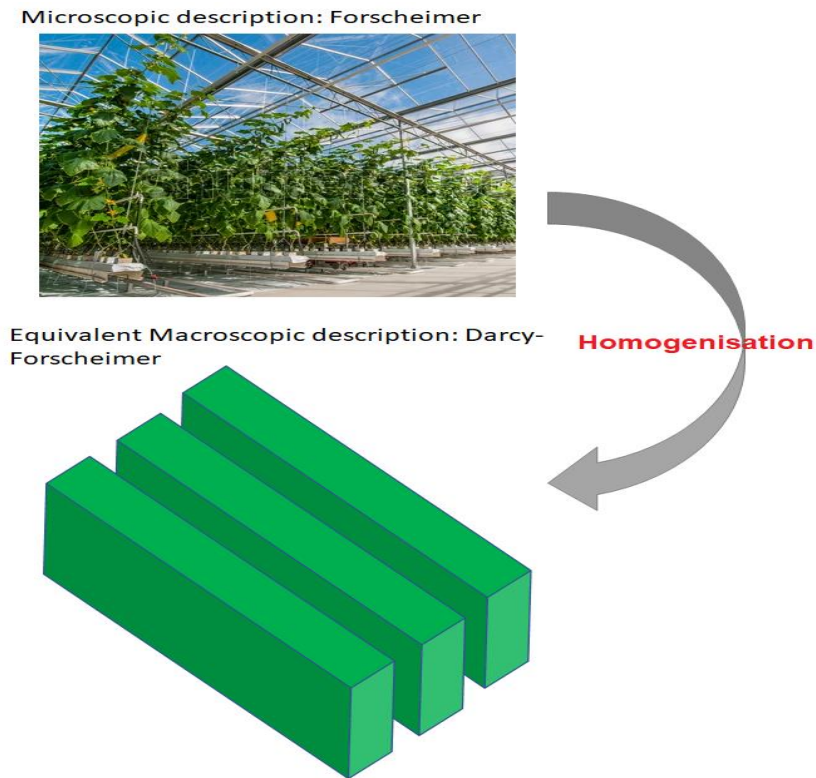
296 where  $v$  is the air speed within the crop cover,  $LAD$  is the leaf area density and  $C_D$  is a drag  
297 coefficient. In addition, considering the crop as a porous medium, the pressure drop induced  
298 by the drag effect can also be expressed through the Darcy-Forchheimer equation:

$$299 \quad S_\phi = - \left( (\mu/K)v + (C_F/K^{0.5})v^2 \right) \quad (3)$$

300 where  $\mu$  is the dynamic viscosity of the fluid,  $K$  the permeability of the porous medium and  
301  $C_F$  the non-linear momentum loss coefficient. For low air speed values observed inside the  
302 canopy, the first term of Eq. (3) to the right can be neglected compared to the quadratic  
303 one. Combining then Eqs. (2) and (3) yields:

$$304 \quad C_F/K^{0.5} = LADC_D \quad (4)$$

305



307

308 **Fig.1** Description of the crop: homogenisation method

309

310 Consequently, as can be seen in Eq. (4) the only required parameters are the leaf area  
 311 density (LAD) (i.e. leaf area divided by the canopy volume), which needs to be measured,  
 312 and the discharge coefficient  $C_D$  which value depends on the considered plant distribution.  
 313 A value of 0.30 for  $C_D$  was calculated by Green (1992) for a forest tree and of 0.20 was  
 314 proposed by Bruse (1995) for plants associations in general. More recently, various  
 315 greenhouse crops were installed in wind tunnel facilities to deduce their discharge  
 316 coefficient. Thus, Haxaire (1999), Lee et al. (2006) and Sase et al. (2012), reported tomato  
 317 crop drag coefficients of 0.32, 0.26 and 0.31 respectively, while Molina-Aiz et al. (2006)  
 318 found  $C_D$  values of 0.26, 0.23, 0.23, and 0.22 for tomato, bell pepper, eggplant, and bean,  
 319 respectively, suggesting that the effect of leaf shape and size is not significant on the drag  
 320 coefficient.

321 **2.3. Sensible heat and water vapour exchanges between plants and air**

322 **2.3.1. Energy balance equation of crops**

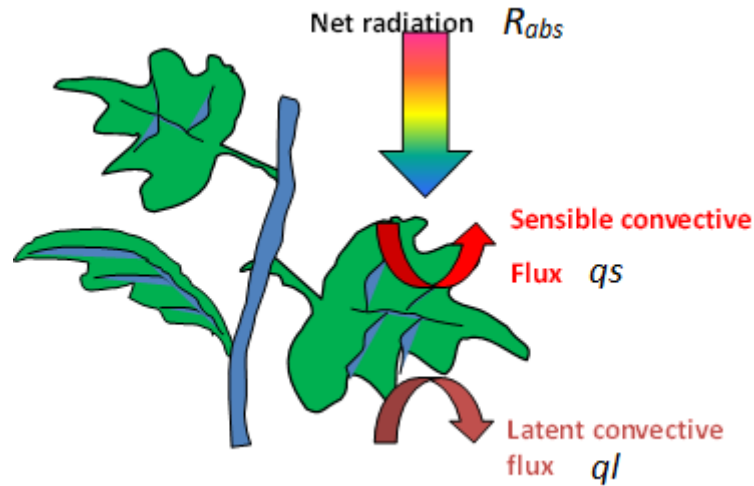
323 In addition to their influence on airflow, plants also significantly alter the overall  
324 energy and water vapour balances. Beyond considering the crop as a sink of momentum, it  
325 must also be considered as a volumetric source or sink of latent and sensible heat.

326 The constraints due to the complexity of crop geometry has led to adopt a  
327 macroscopic approach to describe the crop effects (Fig. 1). Thus, one can establish an  
328 energy balance equation for each elementary volume of the crop. According to this energy  
329 balance, the net radiation absorbed by the crop is equal to the latent and sensible heat  
330 exchanged (Fig. 2).

331 Due to the net radiation  $R_{abs}$  intercepted by plant leaves (mainly owing to solar  
332 radiation during the day), they exchange sensible ( $qs$ ) and latent heat ( $ql$ ) with the  
333 surrounding air. As Brown and Covey (1966) estimated that the heat stored in crops is less  
334 than 1%, the capacitive term of the energy equation is neglected, and the energy balance  
335 equation can therefore be expressed in a simplified way as:

336 
$$R_{abs} + ql + qs = 0 \quad (5)$$

337



338

339 **Fig. 2.** Net radiation, sensible and latent heat balances of leaves

340

341 The crop stands (crop rows) in the greenhouse are represented by parallelepipeds  
 342 arranged in  $n$  rows of length  $L$ , width  $l$  and average height  $H$ , characterised by their  
 343 volumetric leaf area index  $LAD$  linking their leaf surface to their crop volume.

344 The energy balance equation of a volume element  $dV$  becomes:

$$345 \quad R_{abs} - L_v E - 2 LAD C = 0 \quad (6)$$

346 where  $R_{abs}$  is the absorbed net radiation ( $\text{W m}^{-3}$ );  $L_v E$  is the latent heat flux density ( $\text{W m}^{-3}$ ),  
 347  $L_v$  being the heat of vaporisation of water ( $2440 \cdot 10^3 \text{ J kg}^{-1}$  at  $20^\circ\text{C}$ ) and  $E$ , the evaporated  
 348 water flux ( $\text{kg m}^{-3} \text{ s}^{-1}$ );  $C$  is the sensible heat flux density ( $\text{W m}^{-3}$ ). The absorbed radiation  
 349  $R_{abs}$  ( $\text{W m}^{-3}$ ) in each cell of the canopy can be directly deduced from Beer's law, as  
 350 described in Bouhoun Ali et al. (2017).

351 The sensible heat flux is evacuated by both sides of the leaf, hence the presence of a  
 352 coefficient 2 in Eq (6) while the transpiration occurs mainly through the underside of the  
 353 leaf (hypostomatic), however some plants transpire on both sides (amphistomatic leaves)  
 354 like those of tomatoes (see Boulard et al., 1991) which upper side stomatal resistance is  
 355 about 3 times higher than the lower one (equivalent to 3 times less stomatal apertures).

356 The sensible heat flux density  $C$  ( $\text{W m}^{-3}$ ) corresponds to the convective exchanges between  
357 leaves and surrounding air and can be written as follows:

$$358 \quad C = \rho C_p \frac{T_l - T_a}{r_a} \quad (7)$$

359 where  $C_p$  is the specific heat at constant pressure ( $\text{J kg}^{-1} \text{K}^{-1}$ );  $\rho$  is the air density ( $\text{kg m}^{-3}$ );  
360  $T_l$  is the leaf temperature (K),  $T_a$  is the air temperature (K) and  $r_a$  the aerodynamic  
361 resistance ( $\text{s m}^{-1}$ ).

362

### 363 **2.3.2. Leaf transpiration**

364 Ecophysiological transpiration models classically assume that the transfer of water  
365 vapor between the plant and the atmosphere follows a diffusion law proportional to the  
366 water vapor concentration gradient between leaf and ambient air. The total resistance  
367 between inside leaves and air is considered as the sum of two resistances in series (Fig. 3):

368 - the aerodynamic resistance  $r_a$  ( $\text{s m}^{-1}$ ) between the ambient air and the leaf surface.

369 - the stomatal resistance  $r_s$  ( $\text{s m}^{-1}$ ) between the sub-stomatal cavities and leaf surface.

370 Simulating transpiration with this approach thus requires determining leaf temperature in  
371 addition to the physical air and crop parameters.

372 To overcome this problem, another approach proposed by Penman (1948), and later  
373 modified by Monteith (1973), avoids considering leaf temperature to deduce transpiration  
374 according to more easily accessible physical quantities: the radiation absorbed by the  
375 canopy and the air vapour pressure deficit (Katsoulas and Stanghellini, 2019).

376 The latent heat density (transpiration rate density) is given by Eq. 8:

$$377 \quad L_v E = \frac{R_{abs} + 2\rho LAD C_p VPD_a / r_a}{\Delta + 2\gamma \left(1 + \frac{r_s}{r_a}\right)} \quad (8)$$

378 where  $\gamma$  is the psychrometric constant ( $\text{Pa K}^{-1}$ ),  $VPD_a$  is the air-air vapor pressure deficit  
379 (Pa), and  $\Delta$  is the slope of the saturated water vapor pressure curve according to

380 temperature. Yet, as it is based on an approximation of the slope of the water vapour  
381 saturation curve, the leaf temperature has to be close to air temperature, which is not the  
382 case with dry and hot air.

383 All these approaches are based on the concept of the "big leaf", a large virtual leaf  
384 with the average properties of the canopy leaves, both from the climatic, stomatal, and  
385 aerodynamic conductance point of views. Although simplified, this virtual leaf concept has  
386 allowed the development of many transpiration models for a wide range of greenhouse  
387 crops: cucumber (Yang, 1995), rose and various horticultural crops (Baille et al., 1994 a,  
388 b), tomato, (Stanghellini, 1987; Boulard et al., 1991; Fatnassi et al., 2003, 2015; Bartzanas  
389 et al., 2004; Fidaros et al., 2010; Majdoubi et al., 2009, 2016; and Kim et al., 2021a, 2021b).  
390 Ornamental plant interactions with local environment in greenhouses were also studied by  
391 Fatnassi et al. (2006) for roses, by Kichah et al. (2012) and Bouhoun Ali et al. (2018) for  
392 New Guinea Impatiens and by Chen et al. (2015) for Begonia.

393 If one considers leaf temperature  $T_l$ , the water vapor flux between plants and air,  $E$  in  
394  $\text{kg m}^{-2} \text{K}^{-1}$ , can be expressed as follows:

$$395 \quad E = \rho L A D \frac{\omega_l - \omega_a}{r_t} \quad (9)$$

396 Where  $\omega_l$  represents the absolute saturating humidity at leaf level and  $\omega_a$  the absolute  
397 humidity of surrounding air in  $\text{kg kg}^{-1}$ ,  $r_t$  is the total resistance ( $r_s + r_a$ ) to water vapour  
398 (Lhomme and Katerji, 1991).  $\omega_a$  is deduced from the solution of the species transport  
399 equation for the water vapour mass fraction. A recall of classical aerodynamic ( $r_a$ ) and  
400 stomatal ( $r_s$ ) resistance settings is provided in Appendix A.

401

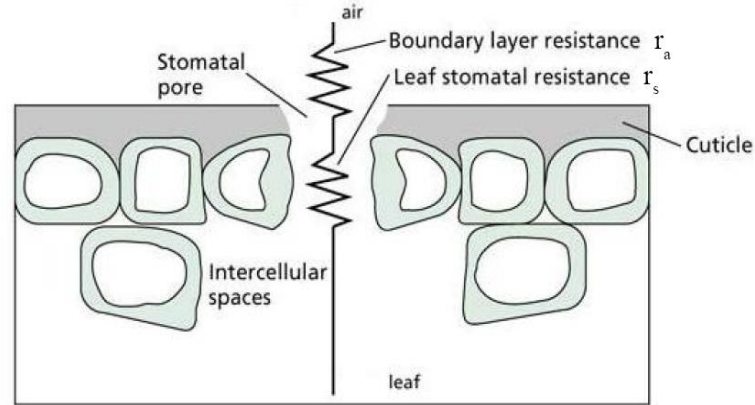


**Fig. 3.** Resistances to water vapor transfer between leaf and air.

#### 2.4. Radiative transfers within the crop equivalent porous medium

The equivalent porous medium is a very flexible and versatile phenomenological approach that allows to consider not only the convective transfers but also the radiative ones. Thus, the canopy is considered as homogeneous and characterised by its extinction coefficient  $K_c$  and the incident global radiation follows a classical Beer-Lambert's law through the crop stands:

$$Rg(z) = Rg_0 e^{-K_c LAD z} \quad (10)$$

where  $Rg(z)$  is the global radiation along the optical path of the sun at a distance  $z$  from the top of the canopy,  $Rg_0$  is the global radiation intercepted at the top of the crop cover,  $K_c$  is the radiation extinction coefficient which depends on the crop (Goudriaan, 1977; Guyot, 1999).

In the first greenhouse CFD studies, the solar distribution was inferred using simple models to determine the distribution of solar radiation within a greenhouse tunnel based on the path of the sun, greenhouse geometry, cover transmittance and sky conditions (Boulard and Wang 2002). Then most authors applied the Beer's law (Bartzanas et al., 2004; Fatnassi et al., 2006; Majdoubi et al., 2009) by providing the incident radiation at the top of the crop and an extinction coefficient within the crop cover to compute the vertical attenuation of

421 solar radiation inside the canopy. It is the reason why they have mainly considered  
422 simulations when the sun was almost at zenith, i.e. around the solar noon and the summer  
423 equinox. This approximation is valid when the crops are short, as it is the case for lettuces  
424 (Boulard & Wang, 2002) or impatiens pot plants (Kichah et al., 2012). This simplified  
425 approach made it however difficult to consider the directional nature of the solar radiation.  
426 Thanks to an appropriate UDF accounting for the directional property of direct solar  
427 insolation, Nebbali et al. (2012) were the first to consider global radiation penetration inside  
428 the canopy on a very realistic way for a tomato crop in a tunnel greenhouse (Fig. 8). They  
429 numerically deduced the solar radiation distribution inside tomato stands but they did not  
430 undertake experimental validation of their model extinction coefficient within the crop  
431 cover and assuming a vertical transfer. Unfortunately, their UDF lacks genericity and could  
432 hardly be reusable for other greenhouses and crop types.

433 More realistic results were obtained by simultaneously solving the radiative transfer  
434 equation (RTE) and convective heat transfer equation. The main difficulty, however, arose  
435 from the nature of the radiative transfers that involve surface-to-surface interactions and  
436 may differ from one wavelength to another for a given medium. The discrete ordinate (DO)  
437 method is often used since it offers a good compromise between accuracy, computational  
438 economy and flexibility. Moreover, it was adapted in commercially available codes such  
439 as Ansys Fluent to take account of the variation of the optical properties of the cover  
440 according to the wavelength range. The main difficulty is that accounting for radiative  
441 transfers requires specific developments. In recent studies, the spectral intensity radiation  
442 within the air was determined by solving the radiative transfer equation (RTE) using the  
443 DO radiation model (Ansys-Fluent, 2010) divided into 2 bands where the radiative and  
444 optical parameters are considered as constants: from 0.4 to 2.4  $\mu\text{m}$  for solar radiation and



445 from 2.4 to 180  $\mu\text{m}$  for terrestrial long wave radiation (Bournet et al., 2007; Nebbali et al.,  
446 2012).

447 The model was then improved by solving the radiative transfer equations using the  
448 same model (DO) within the whole studied domain including the crop cover (Boulard et  
449 al., 2017). In this prospect, the canopy was considered, as a semi-transparent medium with  
450 optical properties adequately expressed in terms of coefficients of extinction and refractive  
451 indexes compatible with the use of the DO radiative application (see Appendix C of  
452 Boulard et al., 2017). Considerable efforts still need however to be done to include the  
453 interchange of short and long wavelength radiation between the sky and the greenhouse  
454 cladding, and between greenhouse structural elements (roof, screens, structural elements,  
455 shelves, canopy...).

## 456 **2.5. Condensation on leaves**

457 As condensation of liquid water on greenhouse crop leaves is responsible for the  
458 development of major fungal diseases like grey mould (*Botrytis C.*) which strongly devalue  
459 the yields (Nicot & Baille, 1996), the study of this mechanism has recently stimulated  
460 several simulation studies based on a CFD modelling approach, particularly for  
461 Mediterranean and Chinese solar greenhouses (CSG) where this question is recurrent.  
462 Basically, it also requires a module of condensation, based on similar aerodynamic  
463 resistance of leaves than previously presented. Condensation risks generally first occur  
464 along roofs and walls that may become colder than inside air or leaves due to radiative  
465 losses at night. Condensation involves a water uptake from the ambient air along the wall  
466 and roof surface, and then on the leaves (which are generally colder than the ambient air),  
467 which occurs when the local temperature goes below the dew point. In CFD model, it is  
468 expressed as a mass flux sink term in the water vapour transfer equation. A thorough

469 description of the condensation model may be found in Bouhoun Ali et al. (2014). The total  
470 rate of mass condensation flux is calculated from Bird et al. (1960) and the corresponding  
471 UDF was adapted from Bell (2003). Piscia et al. (2012) studied the response of a CFD  
472 model to a step-change in night-time transpiration from the crop. The previously mentioned  
473 studies mainly focused on condensation risks on walls and roofs, and it is only recently that  
474 Liu et al. (2021) developed a CFD model to study the spatial and temporal distribution of  
475 the indoor microclimate and condensation on cucumber leaves in a CSG at night. An et al.  
476 (2022) also considered a CSG but for tomato plants and carried out a similar approach for  
477 both diurnal and nocturnal conditions.

## 478 **2.6. CO<sub>2</sub> exchange between plants and air**

479 Due to photosynthesis and respiration, CO<sub>2</sub> is exchanged by leaves with atmosphere  
480 through stomata in the same way as for the water vapour exchange. So, these processes  
481 have been modelled by considering the absorption or production of CO<sub>2</sub> of plants as sink  
482 or source term  $S\phi$  in Eq. (1) where the state variable is the [CO<sub>2</sub>] instead of [H<sub>2</sub>O].

483 Roy et al. (2014) have used a UDF to include a photosynthesis model of the  
484 absorption or production of CO<sub>2</sub> (Thornley, 1976) produced by the plants in a semi-closed  
485 greenhouse with a tomato crop and CO<sub>2</sub> supply. For their simulations, they considered a  
486 3D model of a cropped greenhouse, including a discrete CO<sub>2</sub> injection system and an air-  
487 cooling and dehumidifying system. Comparisons between the simulated and the measured  
488 values of the CO<sub>2</sub> concentration inside the greenhouse were done for a whole day time.  
489 CFD simulations correctly predicted the time course for the net CO<sub>2</sub> consumption per  
490 greenhouse surface unit. Up to now however, to our knowledge, no other work has been  
491 published on that topic although it is of high interest and probably deserves more attention  
492 in the coming years.

493 Several expressions of the photosynthesis process are available as source term,  
 494 Manzoni et al. (2011) expressed it for an elementary crop volume as a multiplicative  
 495 function of light and CO<sub>2</sub> limitation terms, the CO<sub>2</sub> limitation term being obtained by  
 496 linearising the Rubisco limited photosynthesis kinetics; Reichrath et al. (2001) and Molina  
 497 et al. (2017) use the Acock's model which already integrates vertically photosynthesis  
 498 along the entire crop stand profile. Roy et al. (2014) and Boulard et al. (2017) followed the  
 499 model of Thornley (1976) to simulate the absorption or production of CO<sub>2</sub> produced by the  
 500 plants in a semi-closed greenhouse with a tomato crop and CO<sub>2</sub> supply. For their  
 501 simulations, they considered a 3D model of a cropped greenhouse, including a discrete CO<sub>2</sub>  
 502 injection system and an air-cooling and dehumidifying system. They calculated the raw  
 503 photosynthesis flux  $P_r$  for an elementary crop volume, which is more in line with the  
 504 phenomenological approach that considers reduced volumetric elements:

$$505 \quad P_r = \frac{\alpha I \tau \rho C_a}{\alpha I + \tau \rho C_a} LAD \quad (11)$$

506 where  $\alpha$  is the photosynthesis efficiency ( $\alpha=1.01 \cdot 10^{-10} \text{ kg CO}_2 \text{ J}^{-1}$ );  $I$  ( $\text{W m}^{-2}$ ) is the PAR  
 507 incident radiative flux,  $\tau$  is the leaf conductance ( $1/(r_a+r_s)$ ), and  $C_a$  is the concentration of  
 508 CO<sub>2</sub> in surrounding air. It is worth noticing that with respect to water vapour transfers, the  
 509 resistances to CO<sub>2</sub> transfer must be corrected, based on the difference of diffusivity in air  
 510 between CO<sub>2</sub> and H<sub>2</sub>O (Manzoni et al., 2011) with:  $r_{sc}=1.65r_{sw}$  and  $r_{ac}= 1.34r_{aw}$  ; the  
 511 subscripts  $c$  and  $w$  refer to CO<sub>2</sub> and H<sub>2</sub>O respectively.

512 The production of CO<sub>2</sub> consists in the maintenance and growth respirations which together  
 513 can be estimated for tomato crop to 22% of the raw photosynthesis consumption (see  
 514 complementary details in Boulard et al. (2017)), hence the net photosynthesis consumption  
 515 flux  $S_{CO_2}$  is:

$$516 \quad S_{CO_2} = 0.78P_r \quad (12)$$

517

### 518 **3. Numerical implementation**

#### 519 **3.1. UDF description**

520 Thanks to the possibility to customise CFD software, heat and mass exchanges  
521 between the plant and the greenhouse air are introduced in the CFD model through the  
522 addition in equation 1 of source/sinks terms describing these transfers. Following Boulard  
523 & Wang (2002), each mesh of the crop cover is simulated to a “volume heat source” of  
524 porous medium absorbing a radiative flux,  $R_{abs}$  (Eq. 10). This flux is partitioned into  
525 convective sensible ( $q_s$ ) and latent ( $q_l$ ) heat fluxes (water vapour) according to Eq. (5),  
526 which themselves depend on the aerodynamic ( $r_a$ ) and stomatal ( $r_s$ ) and resistances  
527 between the virtual solid matrix representing the crop and the local climate characterised  
528 by air ( $T_a$ ) and leaf ( $T_l$ ) temperatures and absolute humidity ( $\omega_a$ ).

529 The expression of the latent heat flux requires the calculation of the water vapour  
530 concentration  $\omega_l$  which can be obtained from the leaf temperature  $T_l$  according to the  
531 Magnus Tetens law for the saturated water vapour pressure:

$$532 \quad \omega *_{T_l T_l} = 610.5 e^{(17.269 T_l / 237.3 + T_l)} \quad (13)$$

533 As  $r_a$  and  $r_s$  depend on the local climate (but also on the plant substrate water status (see  
534 Appendix A), a close coupling between the crop and air flow is thus operated. Finally, we  
535 get a system of two equations with two unknowns which are additional outputs of great  
536 interest, determined into each mesh of the crop cover: the leaf temperature ( $T_l$ ) and ( $\omega_l$ ) the  
537 latter allowing to deduce the value of the latent heat flux associated with the transpiration  
538 of the cover  $E$  following Eq. (9).

539 CFD software makes it possible to specify the above mentioned latent and sensible  
540 heat fluxes as source terms for the conservation equation (Ansys-Fluent (2010)). Source

541 type boundary conditions are then applied to each crop row to simulate plant activity. To  
542 describe the source term  $S_{\phi}$  of the conservation equation, CFD software such as Fluent  
543 Ansys<sup>TM</sup> uses most of the time a relationship of the form:

$$544 \quad S_{\phi} = A + B \cdot \phi \quad (14)$$

545 where  $A$  and  $B$  must be identified regarding to the volumetric latent and sensible heat  
546 expressions provided by Eqs (7) and (8).

547 For the temperature:

$$548 \quad A = \frac{2 * LAD \rho C_p}{r_a} T_l \text{ and } B = - \frac{2 * LAD \rho C_p}{r_a} \quad (15)$$

549 For the water vapor content:

$$550 \quad A = \frac{LvLAD \rho C_p}{(r_a + r_s)} \omega_l \text{ and } B = - \frac{LvLAD \rho C_p}{(r_a + r_s)} \quad (16)$$

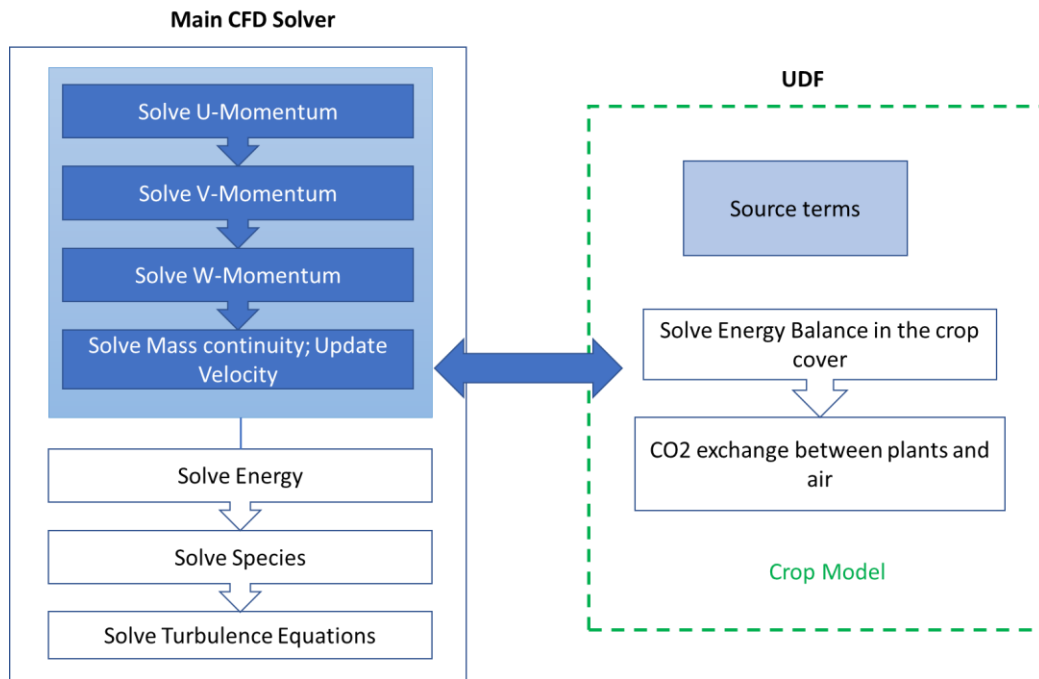
551 The equations describing  $r_s$  (see Appendix A) are also solved by means of a UDF specially  
552 developed for this purpose and coupled with the main CFD solver which provides the local  
553 climate parameters within each mesh (Figure 4). The connection between the crop  
554 submodel routine and the main solver is described in Fig. 4.

555 The output of the crop submodel is the leaf temperature which is deduced from the energy  
556 balance over the crop by combining Eqs (6), (7) and (8):

$$557 \quad T_l = \frac{r_a}{2LAD \rho C_p} (R_{abs} - ql) - T_a \quad (17)$$

558

559



560

561 **Fig. 4** Sketch of the exchanges between the UDF and the main solver in the CFD model.

562 **3.2. Mesh and boundary conditions**

563 Following Boulard & Wang (2002), the calculation domain includes most of the time  
 564 the greenhouse and its close environment (Fatnassi et al., 2003, 2006; Majdoubi et al., 2009,  
 565 2016; Nebbali et al., 2012), but it can sometimes be restricted to the inside volume of the  
 566 greenhouse if the boundary flow conditions at the greenhouse surface are known (Kichah  
 567 et al., 2012; Boulard et al., 2017; An et al., 2022). Inside the greenhouse, the crop stand is  
 568 considered as a porous medium, with the same geometry and dimensions as in reality.

569 If the calculation domain includes the greenhouse and its close environment, an inlet  
 570 logarithmic velocity profile or power law profile corresponding to the measured wind  
 571 profile is generally imposed at the entrance of the calculation domain, along with the air  
 572 temperature, and water mass fraction values (and  $[CO_2]$  concentration if necessary). The  
 573 radiative flux is also imposed at the upper limit of the calculation domain. At the outlet of  
 574 the calculation domain, all variable gradients are generally set to zero, except for the

575 pressure. The temperature of the walls, roof, and soil surfaces are deduced from an energy  
576 balance over these surfaces.

577 The computational grid is refined near solid boundaries i.e. soil, walls, and roof where  
578 stronger gradients of the variables of interest (velocity, temperature...) are expected. Tests  
579 of independency of the grid regarding the results are generally undertaken to optimise the  
580 cell numbers and distribution with the aim to limit the required CPU time to get a reliable  
581 solution.

### 582 **3.3. Validation of CFD model**

583 The validation of the CFD model is generally conducted through the comparisons of  
584 computed and measured greenhouse climate fields (air temperature and humidity but also  
585 sometimes CO<sub>2</sub> concentration, wall and ground temperatures, leaf temperature) or flux  
586 measurements (air speed, crop transpiration, condensation fluxes, radiation) as well as  
587 global air exchange rates (Table 1). The first validations were performed using state  
588 variables such as air speed, air, and leaf temperatures (Haxaire, 1999) for tomato crop and  
589 transpiration fluxes (Boulard & Wang, 2002) for lettuce crop. Later, Fatnassi et al. (2002,  
590 2003, 2015) and An et al. (2022) have used networks of sensors to monitor temperature and  
591 humidity in horizontal and vertical plans inside the greenhouse. Recently, Boulard et al.  
592 (2017) mapped CO<sub>2</sub> and Liu et al. (2021) water condensation on the plastic roof and  
593 cucumber leaves with similar 3D validation approach. Thanks to the existence of stable  
594 wind regimes like *Mistral* in the lower Rhone valley or coastal winds on the Moroccan  
595 Atlantic shore, one can also displace the sensors all along the greenhouse volume to map  
596 air temperature or humidity while normalising the measured values with respect to outside  
597 wind, which is the main driving force of greenhouse ventilation (Haxaire, 1999; Majdoubi  
598 et al., 2009). All these measurements have been confronted to simulated data and they

599 generally confirm the accuracy of the model to produce the microclimatic flow fields inside  
 600 the greenhouse, including the crop stands.

601

602 **Table 1.** Validation studies of the CFD model based on the comparison between measured  
 603 and simulated values of climate parameters in the greenhouse

<b>Authors</b>	<b>Greenhouse type</b>	<b>Crop</b>	<b>Dimension</b>	<b>Validation</b>
Boulard & Wang (2002)	Tunnel	Lettuce	3D steady	Transmittance, air velocity Temperature, transpiration flux
Fatnassi et al. (2003)	Moroccan type	Tomato	3D steady	Ventilation rate
Bartzanas et al. (2004)	Tunnel	Tomato	2D/3D steady	Air velocity, ventilation rate, air temperature
Fatnassi et al. (2006)	Multi span	Roses	3D steady	Ventilation rate
Majdoubi et al. (2009)	Canary type	Tomato	3D steady	Air temperature, relative humidity
Tong et al. (2009)	Chinese	Lettuce	2D unsteady	Air temperature
Boulard et al. (2010)	Multispan plastic	Roses	2D unsteady	Air temperature and humidity, spore concentration
Piscia et al. (2012a)	4-span plastic	Lettuce	3D unsteady	Air temperature, roof temperature, humidity ratio
Tamimi et al. (2013)	Arch type	Tomato	3D steady	Air velocity, evapotranspiration, stomatal resistance
Majdoubi et al. (2016)	Canarian	Tomato	3D steady	Air temperature and humidity
Bouhoun Ali et al. (2018)	Venlo glass house	New Guinea Impatiens	2D unsteady	Air temperature, leaf temperature matric potential, stomatal resistance, air humidity, transpiration rate
Boulard et al. (2017)	6-span glasshouse	Tomato	3D unsteady	Air temperature, leaf temperature, saturated humidity at leaf temperature, air humidity, shortwave radiation, air speed, crop transpiration, CO <sub>2</sub> concentration
Bouhoun Ali et al. (2019)	Venlo glass house	New Guinea Impatiens	2D unsteady	Air temperature and humidity, stomatal resistance, ventilation rate
Fatnassi et al. (2021)	Four-span plastic arched greenhouse	Rose	3D unsteady	Air temperature and humidity

604

## 605 **4. Main results from CFD studies including a crop submodel**



606 Following the pioneer works of Haxaire (1999) and Boulard and Wang (2002),  
607 Bartzanas et al. (2004), Fatnassi et al. (2003, 2015), Fidaros et al. (2010), Majdoubi et al.  
608 (2009, 2016), An et al. (2021) developed CFD simulations with crop sub-models,  
609 principally for tomatoes but also for cucumber (Liu et al., 2022). Ornamental plant  
610 interactions with local environment in greenhouses was also studied by Fatnassi et al.  
611 (2006, 2016) for roses, Kichah et al. (2012) and Bouhoun Ali et al. (2018, 2019) for New  
612 Guinea Impatiens and by Chen et al. (2015) for Begonia.

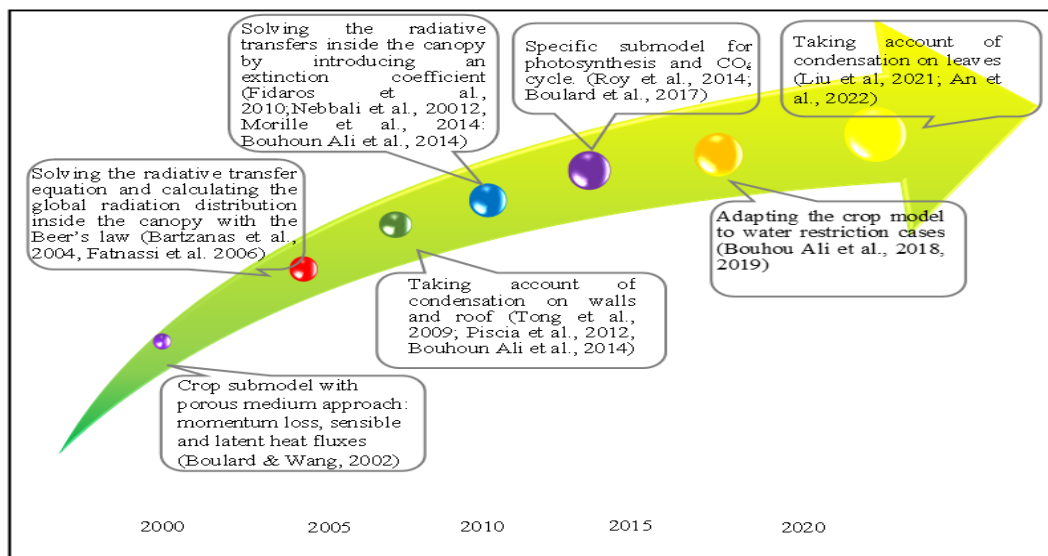
#### 613 **4.1. Milestones of CFD crop model developments**

614 Figure 5 depicts the milestones of crop model developments. Since the pioneering  
615 works of Boulard & Wang (2002) who included both the momentum sink terms and the  
616 sensible/latent source terms in the conservation equations for water mass fraction,  
617 momentum, and energy, several improvements of the model have been undertaken. This  
618 model was recently adapted to consider the simulations of the crop behaviour under  
619 suboptimal water inputs that may lead to stomatal partial closing and transpiration rate  
620 reductions, as is often the case in real situations (Bouhoun Ali et al. 2018, 2019).

621 Radiative transfer within the crop itself is still a major concern since it determines the  
622 two main physiological crop functions: transpiration and photosynthesis. The  
623 determination of the global radiation in each cell is therefore required. It was first assessed  
624 from the application of the Beer's law (Fanassi et al. 2003; Bartzanas et al. 2004, Fatnassi  
625 et al., 2006, Majdoubi et al., 2009) knowing the incident global radiation at the top of the  
626 canopy, before improvements were made by solving the Radiative Transfer Equation (RTE)  
627 first in the domain surrounding the crop, and then inside the crop itself (Fidaros et al., 2010;  
628 Nebbali et al., 2012; Morille et al., 2013; Bouhoun Ali et al., 2018, 2019).

629 CO<sub>2</sub> exchanges and photosynthesis were included in CFD models by Roy et al. (2014)  
 630 and Boulard et al. (2017) who have considered the absorption or production of CO<sub>2</sub> by the  
 631 plants in their models.

632 In parallel, a special attention was paid to include condensation process in the  
 633 simulation through a specific subroutine determining the water uptake from the air and  
 634 corresponding heat flux along the walls and roofs (Tong et al., 2009; Piscia et al., 2012a,  
 635 b; Bouhoun Ali et al., 2014), but it is only very recently that condensation potentially  
 636 occurring along the leaves was introduced in the CFD approach (Liu et al., 2021, An et al.,  
 637 2022).



638  
 639 **Fig. 5** Milestones of CFD crop submodel developments

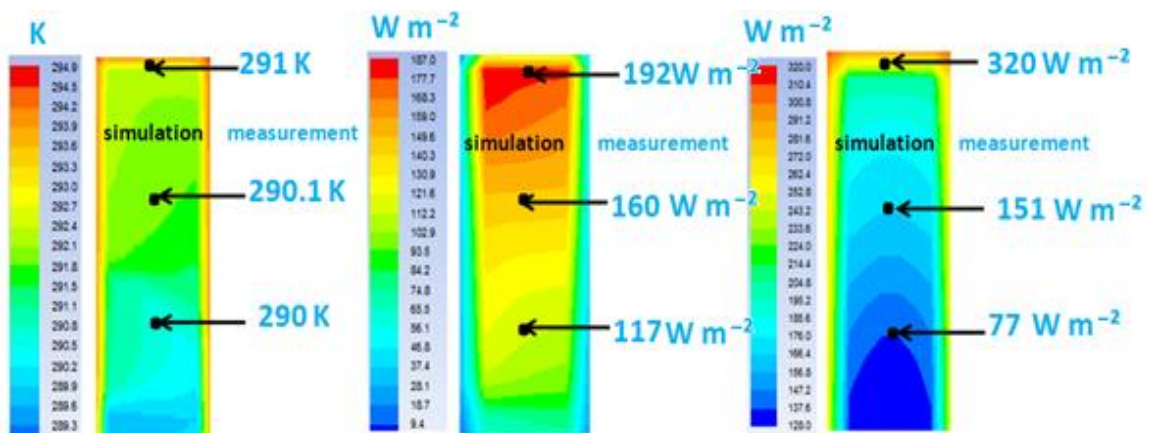
640 **4.2. Distribution of leaf temperature, crop transpiration and shortwave radiation**  
 641 **inside the crop**

642 Following the progress in CFD modelling, simulations gained in accuracy and made  
 643 it possible to assess interactions of the crop with the local environment into details.  
 644 Pouillard et al. (2012) have considered an experimental closed greenhouse with a tomato  
 645 crop to assess the radiation distribution inside the greenhouse including the crop stands.

646 They solved the radiative transfer equation, using the Discrete Ordinate model with a proper  
 647 parameter setting concerning the optical properties of the semi-transparent medium  
 648 simulated to the porous medium and distinguishing short from long wave radiations.  
 649 Implementing a crop submodel encapsulated in a UDF dynamically linked with the main  
 650 solver, they simulated the distribution of leaf temperature, air temperature and crop  
 651 transpiration within the crop based on air velocity and surrounding climate parameters (Fig.  
 652 6).

653 Their results evidenced that the heterogeneity of the climate inside the greenhouse  
 654 affects plant activity as illustrated in Fig. 6 showing the distributions of leaf temperature,  
 655 crop transpiration and short waves radiations received within a tomato plant stand. They  
 656 also showed that for this greenhouse, at the upper part of the crop stand, 2/3 of the captured  
 657 radiative energy was transferred to latent heat thus increasing air humidity while only the  
 658 remaining part contributed to greenhouse air warm up and heat accumulation higher. They  
 659 also predicted that in the middle and lower parts of the crop, the latent heat associated with  
 660 transpiration was higher than the received radiative energy, meaning that the leaves cooled  
 661 the air at these levels.

662

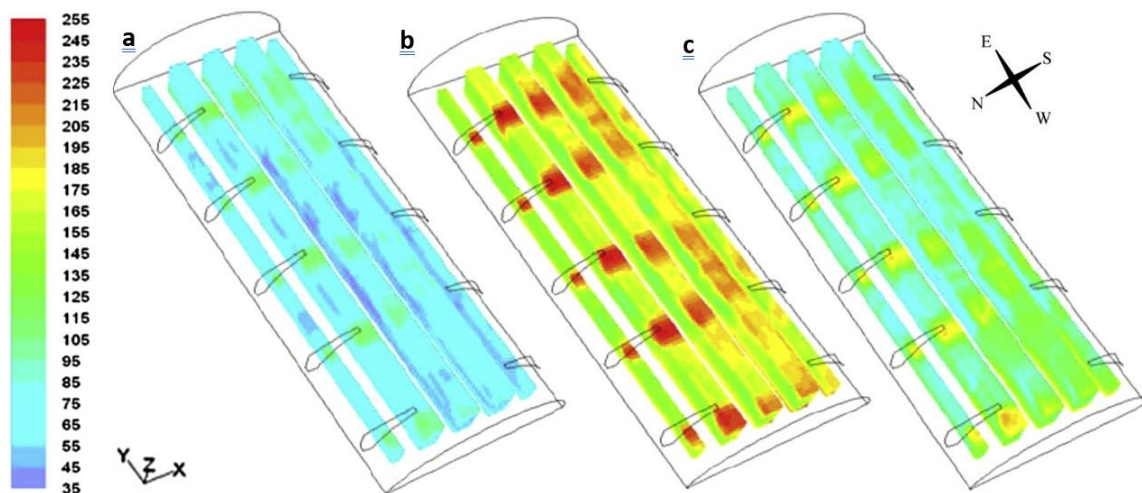


663

664 **Fig. 6** Simulated and measured distributions of leaf temperature in K (left), latent heat of  
665 crop transpiration in  $W m^{-2}$  (middle) and short waves radiations in  $W m^{-2}$  (right)  
666 within the crop cover at noon (after Pouillard et al., 2012).

667 Using the same approach and implementing a module of solar transmission inside the crop  
668 cover, Nebbali et al. (2012) got very realistic results (Fig. 7), making it possible to assess  
669 the heterogeneity of crop transpiration and its evolution with the sun path all day long.  
670 Nevertheless, they did not undertake any validation of their model against experimental  
671 data.

672



673

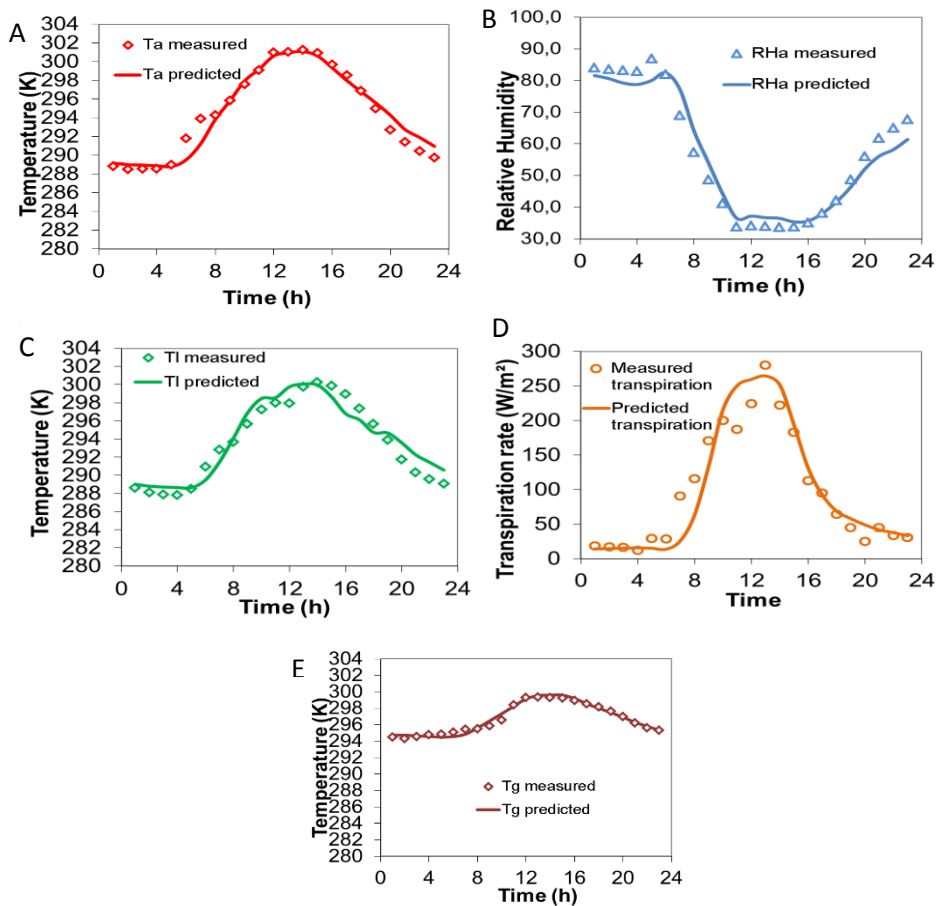
674 **Fig. 7** Distribution of the transpiration heat flux density on June 21<sup>st</sup>. (a): at sunrise,  
675 (b): at midday, (c): at sunset (after Nebbali et al., 2012).

676

677 Bournet et al. (2017) carried out two-dimensional unsteady simulations at a daily  
678 timescale including crop interaction and sun path. The radiative transfer equation (RTE)  
679 was solved, based on the Discrete Ordinates method distinguishing short and long  
680 wavelength radiations. The ground was also meshed to simulate conduction. The model  
681 was run for a typical sunny day under temperate climatic conditions and validation was  
682 undertaken based on seven different parameters including temperature and relative

683 humidity of the air above and inside the crop, ground temperature, leaf temperature and  
 684 transpiration rate (Fig. 8). Simulations stress the ability of the model to correctly predict  
 685 the response of the greenhouse to a variation of the outside climate. In particular, the strong  
 686 influence of the solar radiation was demonstrated. Although leaf temperature and  
 687 transpiration rate were satisfactorily simulated, as well as local air humidity and  
 688 temperature just above the canopy. The air temperature inside the canopy was however a  
 689 little bit overestimated, and humidity underestimated suggesting that the air movement  
 690 inside the canopy could be overestimated maybe because of an underestimation of the drag  
 691 force of the porous medium.

694  
 695  
 696  
 697  
 698  
 699  
 700  
 701  
 702  
 703  
 704  
 705  
 706  
 707

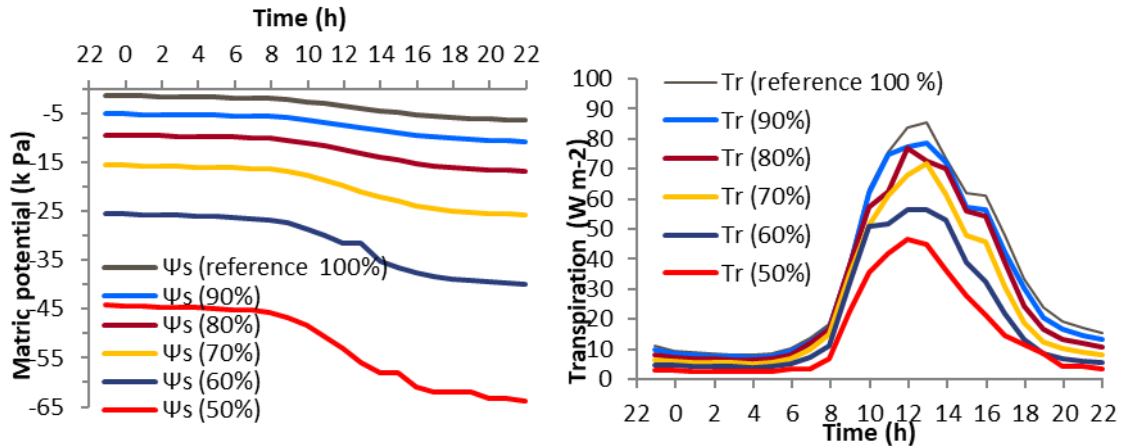


708           **Fig.8** Comparison of measurements and CFD simulations for A) air temperature  
709 above the crop; B) relative humidity above the crop; C) leaf temperature, D) transpiration  
710 rate and E) soil surface temperature (adapted from Bournet et al., 2017).

711

712           Bouhoun Ali et al. (2018) adapted the crop model for cases when plants are subject  
713 to water restriction. In this prospect, they calibrated a multiplicative stomatal resistance  
714 expression depending not only on the meteorological parameters, but also on the soil water  
715 potential (Cannavo et al., 2016) and developed a submodel to calculate the water balance  
716 over the substrate. This model demonstrated its ability to predict the decrease of water  
717 availability in the substrate and that both stomatal resistance, air and leaf temperatures  
718 inside the canopy were higher for the water restricted conditions than for the well-watered  
719 one. It also showed that transpiration rates were lower for plants under water restriction  
720 (Figure 9), due to stomatal partial closing and transpiration rate reduction.

721           The same model was then implemented by Bouhoun Ali et al. (2019) for six different  
722 irrigation regimes, reducing progressively the water inputs. From the simulations, the  
723 scenario with 70% water supply (considering well water plants as the reference) appeared  
724 as a good compromise between the maintenance of plant activity and water saving, together  
725 with a reduction of fungal diseases or mould development risks. CFD simulations could,  
726 hence, improve water management strategy and identify microclimate conditions adapted  
727 to plant growth while reducing water inputs. It must be stated however, that the authors did  
728 not investigate the impacts of water restriction on plant architecture and quality which  
729 condition the marketing criteria.



730

731 **Fig. 9.** Evolution of the matric potential in the ground (a) and corresponding evolution of  
 732 the evapotranspiration predicted by a CFD model for an impatiens crop (b) (after  
 733 Bouhoun Ali et al., 2018)

734 **4.3. Simulation of the distribution of CO<sub>2</sub> concentration in the greenhouse**

735 CFD makes it possible also to investigate the carbon dioxide fluxes associated with the  
 736 photosynthesis and respiration processes. This has allowed mapping the CO<sub>2</sub> and H<sub>2</sub>O  
 737 concentrations in air, together with temperature inside cropped greenhouses often equipped  
 738 with CO<sub>2</sub> injection systems. Reichrath et al. (2001) were to our knowledge the first to be  
 739 interested in including the crop total carbon dioxide uptake rate for photosynthesis in CFD  
 740 modelling. Following Acock's suggestion they divided the crop into three layers and  
 741 showed that the top layer consumes 66% of total carbon dioxide, the middle one 27%, and  
 742 the bottom one only 7%. In their simulations, the carbon dioxide injection and absorption  
 743 by the crop were added to a two-dimensional CFD model and applied to a 60-span Venlo  
 744 type glasshouse. Carbon dioxide dispersion was simulated, and revealed a higher  
 745 concentration at the leeward part of the glasshouse due to less efficient ventilation  
 746 compared to the windward side of the greenhouse (Fig. 10).



747

748 **Fig.10** Carbon dioxide dispersion in a 60 span Venlo-type glasshouse with crops  
 749 (after Reichrath et al., 2001).

750

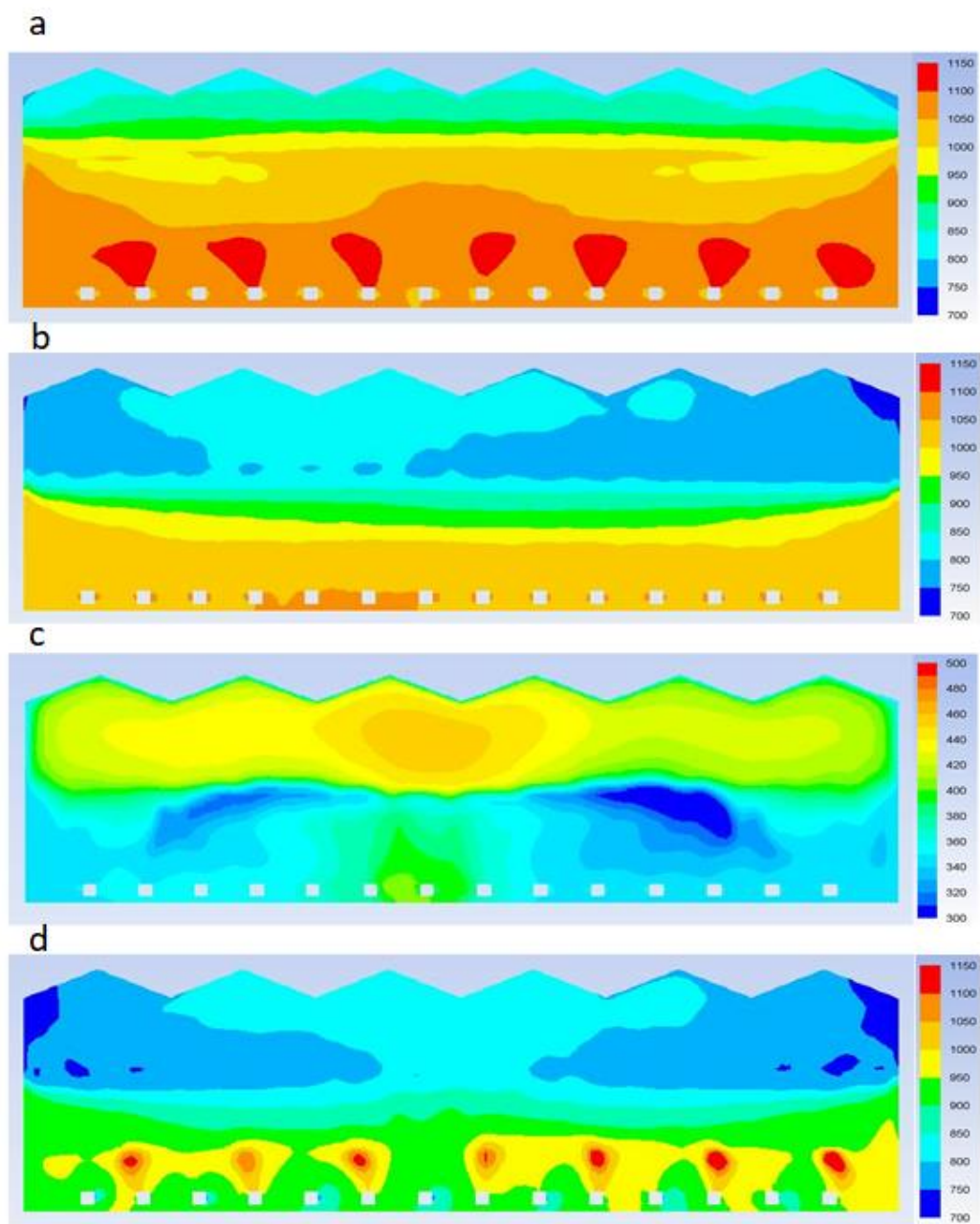
751 More recently, Roy et al. (2014) and Boulard et al. (2017), investigated the 3-dimensional  
 752 distribution of CO<sub>2</sub> in a closed plastic-greenhouse using both numerical, including a CFD  
 753 crop model, and experimental approaches. In their study, the CO<sub>2</sub> concentration was solved  
 754 by adding a transport equation for the CO<sub>2</sub> mass fraction in the 3-D CFD model, and using  
 755 the porous medium approach coupled with crop eco-physiological and radiative transfer  
 756 models. Transpiration and photosynthesis fluxes were considered as a function of this  
 757 concentration and other microclimatic parameters.

758 They could predict the distribution of CO<sub>2</sub> concentrations in the greenhouse at various times  
 759 of the day (Fig. 11, a-d). For example, at 8:00 am the greenhouse was closed, and CO<sub>2</sub> was  
 760 supplied, which corresponds to higher concentration zones appearing near ground and  
 761 injection pipes (Fig. 11a). As the greenhouse was always maintained closed at 11h 30 (Fig.  
 762 11b) CO<sub>2</sub> concentration was still very high at the bottom of crop rows (1200 ppm) near the  
 763 injection pipes. Due to ventilation needs, injection was turned off at 1h pm (Fig. 11c)  
 764 leading to a severe depletion (300 ppm) at crop level, due to an intense uptake for



765 photosynthesis. At 5:30 pm the greenhouse was again closed, and the CO<sub>2</sub> injection was  
766 turned on again (Fig. 11d), leading again to higher concentration zones near the injection  
767 pipes and a strong stratification.

768

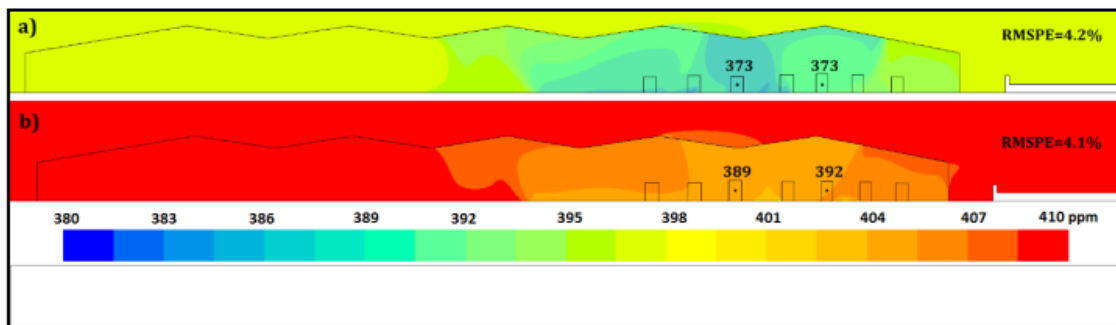


769

770 **Fig. 11.** Simulated carbon dioxide levels (ppm) in a median vertical transverse plane of the  
771 greenhouse at (a) 8:00 am; (b) 11:30 am; (c) 1:00 pm; (d) 5:30 pm. (After Boulard et al.,  
772 2017).

773

774 Molina-Aiz et al. (2017) implemented a CFD model to simulate photosynthesis in an  
775 Almeria-type greenhouse without CO<sub>2</sub> injection by incorporating the Acock's model by  
776 means of UDF's and the modelled CO<sub>2</sub> distribution shows a depletion in the leeward part  
777 of the greenhouse, where are situated the plants which absorb CO<sub>2</sub> (Fig. 12). The  
778 concentration of CO<sub>2</sub> in the windward part of the greenhouse was like the outside value,  
779 indicating that natural ventilation was sufficient to maintain an adequate concentration for  
780 the plants.



781

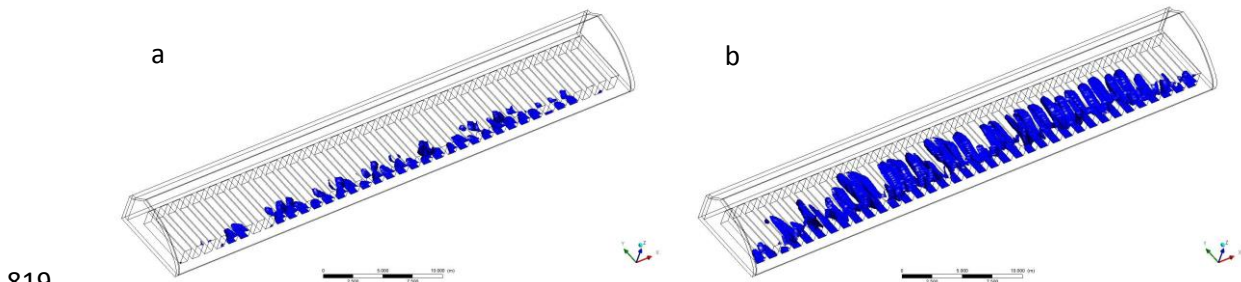
782 **Fig. 12.** Distributions of CO<sub>2</sub> concentration simulated with CFD and measured values  
783 (indicated in the figures) in the greenhouse on (a) 3/11/2014 and (b) 3/13/2014. (After  
784 Molina et al., 2017)

#### 785 4.4. Simulation of condensation

786 Condensation is a key phenomenon in greenhouse management, not only because it may  
787 partly compensate water inputs due to evapotranspiration, thus reducing the water content  
788 of the air and consequently the absolute humidity, but also because condensation enhances  
789 risks of fungal developments or other diseases. To our knowledge, Tong et al. (2009) were  
790 probably among the first to take account of condensation in their CFD approach applied to

791 a closed, empty Chinese Solar Greenhouse. Their numerical model included specific source  
792 terms derived from the formula suggested by Garzoli (1985) for the condensation that  
793 occurred along the walls when the local temperature goes below the dew point. The latent  
794 heat was then applied as an equivalent heat source to the roof where condensation occurred.  
795 A more formalised model based on local steady state balance for the sensible heat and water  
796 vapor was applied by Piscia et al. (2012) to a closed greenhouse. They conducted a  
797 comprehensive analysis of the condensation process during night-time conditions and  
798 determined the water uptake from the air by adapting a specific subroutine developed by  
799 Bell (2003) based on the equation provided by Bird et al. (1960). In their study, however,  
800 Piscia et al. (2012) considered the crop as a constant source of water vapor, thus neglecting  
801 the interaction of the crop with the ambient climatic conditions. Moreover, they determined  
802 the water uptake from the air, but omitted the associated heat flux along the walls. Bouhoun  
803 Ali et al. (2014) conducted a CFD study for an Impatiens New Guinea greenhouse crop in  
804 which water uptake from the ambient air along the roof surface, was expressed as a mass  
805 flux sink term in the water vapor transfer equation. The corresponding source term for the  
806 energy equation could then be obtained by multiplying the mass flux by the latent heat of  
807 vaporisation. In particular, their results revealed the ability of the model to predict both the  
808 air and wall temperatures of the greenhouse. In their recent paper, Liu et al. (2021)  
809 simulated both the distributions of roof condensation and leaf condensation (Fig. 13). The  
810 condensation on the leaves at 9 measurement points was observed manually for comparison  
811 with the simulation results each hour from 18:30 to 5:30. They observed that condensation  
812 always occurred earlier than the simulated condensation. They also reported that  
813 condensation always appeared first on the roof rather than on the leaves. Focusing on the  
814 Leaf Wet Duration (LWD) as an indicator of risk of fungal development, they predicted an

815 average error between the observed and simulated LWD of 1.25 h for the two studied days.  
816 They concluded that the crop canopy condensation model is appropriate to quantify the  
817 dynamics of water vapour and energy, even though, the model is expected to improve  
818 performance in a variety of scenarios.



819  
820 **Fig. 13.** Simulated leaf condensation on April 17 at (a) 01:30 and (b) 05:30. Y represents  
821 the north; X represents the east; and ■ represents the condensation that appeared based on  
822 simulation (after Liu et al., 2021).

## 823 **5. Future trends**

824 Despite the stated advances in CFD based plant activity modelling in greenhouses, further  
825 improvements still have to be conducted to reach a higher degree of realism.

### 826 **5.1. A better consideration of radiation transfer in the crop stands**

827 Given the complexity of radiative transfer into the whole greenhouse, with various light  
828 qualities (short and long waves; diffuse and direct light) interacting with different media  
829 (solid, diopters, transparent, diffuse), numerical simulations must consider the entire range  
830 of these exchanges, particularly between the leaves and other surrounding surfaces. Still,  
831 considerable efforts need to be done to include the interchange of short and long wavelength  
832 radiation between the sky and the greenhouse cladding, and between greenhouse structural  
833 elements (roof, screens, structural elements, shelves, canopy...). Indeed, for most of the

834 existing studies, the radiative transfers were considered less important than the convective  
835 ones and consequently largely simplified, even if the increase in the performance of the  
836 computer facilities and model developments made it possible to considerably improve  
837 radiation considerations in CFD modelling tools and offers new perspectives.

838 In addition, model microclimate validations with respect to light measurements are very  
839 rare, whereas greenhouse plant production directly depends, through photosynthesis and  
840 transpiration, on this parameter. Accordingly, a double effort must be performed (i) on the  
841 adaptation of the available radiation models of the CFD packages to the various radiative  
842 transfers, including inside the equivalent porous medium, and (ii) on the measurements and  
843 validation of light distribution into the greenhouse volume, including the plant stands.

## 844 **5.2. Towards the development of virtual plants under CFD model**

845 With the recent advances in computing capacities, and to reach more realism with the CFD  
846 simulation of the plants, connections should be established with virtual plants that simulate  
847 their real activities, meaning indeed a reinforcement of collaborations between greenhouse  
848 systems modelers and the physiologists community.

849 This should integrate in a fine way the functioning of the plant by introducing more accurate  
850 mechanisms through the 3D construction of the plants. In such approach, photosynthesis  
851 and transpiration will be calculated at the leaf level in the plant architecture according to  
852 its microclimate by a transport-resistance system based on the sources/sinks of the various  
853 organs. As already seen (Bouhoun Ali et al., 2017), plant water and nutrient uptake can also  
854 be included in these augmented reality models (Kim et al. 2021a; 2021b).

### 855 **5.3. Integration of other biotic/non-biotic interferences**

856 Plants are not the only biotic agents interfering with microclimate in greenhouses, thus  
857 fungi, various diseases and insects also directly depend on it and several CFD approaches  
858 have recently been performed towards this global integration. Hence, Boulard et al. (2010)  
859 have developed and validated a CFD prediction of climate, crop activity and fungal spore  
860 transfer in a rose greenhouse, thus showing that both the plants and the airborne transfers  
861 of most pathogens can be catch by this approach. Fatnassi et al. (2022) have developed a  
862 CFD modelling of the microclimate within the boundary layer of leaves in the ecological  
863 niche of most bio-aggressor's and defender's (insects but also fungi and bacteria) to  
864 improve pest control management and define how to turn them unfavourably or favourably.  
865 Liu et al. (2021) have developed a CFD based 3-D simulation of leaf condensation on  
866 cucumber canopy in a solar greenhouse serving as a reference for an early warning model  
867 of diseases based on the temporal and spatial distribution of leaf condensation. Their model  
868 may serve as a reference for an early warning model of disease based on the temporal and  
869 spatial distribution of leaf condensation given that it would be costly to monitor the  
870 condensation of all the leaves in a greenhouse. Discrepancies with experimental  
871 condensation measurements still exist and further developments are required to improve  
872 the model. Furthermore, it will be necessary to cope with the high computational load  
873 required by the model to reach the application of this tool in real-time in greenhouse  
874 production in the next future, which is of great significance for providing disease warning  
875 and guidance in pest control decision-making.

### 876 **6. Conclusions**

877 A description of the different steps of integrating the greenhouse plant activity in  
878 CFD models has been detailed in this paper and particularly the sub-program allowing to  
879 calculate the involved parameters as well as the links connecting them with the main solver.

880 Since the 90s, many CFD models coupling the dynamic effects and mass exchanges  
881 between crop and air inside the greenhouse have been developed. Their systematic  
882 validations show that they predict accurately the distribution of air speed, temperature,  
883 humidity and CO<sub>2</sub> fields inside the greenhouse and the crop rows or canopy. In addition,  
884 they provide very important information on plant activity, often including transpiration and  
885 more seldom photosynthesis and allow to test improvements of the design and equipment  
886 of the greenhouse with respect to crop production.

887 In a context of resources scarcity such as water and energy, this approach  
888 undoubtedly provides comprehensive and easy-to-use tools to tune and optimise the  
889 greenhouse system to increase the yield and quality with a low environmental impact.

890

## Appendix A

891

892

### 893 A.1 Aerodynamic resistance

894 Within the limits of the climatic variations encountered in greenhouses, the  
895 aerodynamic resistance value ( $r_a$ ) is not very much influenced by the variations in the  
896 characteristics of the humid air but depends widely on the air flow regime. Due to the low  
897 values of air speed met in greenhouses generally encountered, Baille et al. (1994)  
898 considered a constant value of  $r_a$  for roses. Nevertheless, several formulas based on local  
899 air speed are proposed in the literature (Roy and Boulard, 2005). For greenhouse tomato  
900 crops and low wind speeds Boulard et al. (2002) applied the following formulation:

$$901 \quad r_a = \frac{\rho_a c_p}{h_s} \quad (A.1)$$

902 where the heat exchange coefficient  $h_s$ , depends on the Nusselt number ( $Nu$ ) and the  
903 flow regime near the leaves.

$$904 \quad h_s = \frac{Nu \lambda_a}{d} \quad (A.2)$$

905 where  $\lambda_a$  is air conductivity ( $\text{W m}^{-1} \text{K}^{-1}$ );  $d$  (m) characteristic dimension of the leaves.

906 Generally, the flow regime near the leaves is widely considered laminar, although  
907 it is turbulent further away from leaves and for a laminar flow,  $Nu$  can then be written  
908 as a function of the convection mode. Assimilating the leaf to a horizontal flat plate  
909 (Monteith and Unsworth, 2013; Morille et al., 2013; Roy et al., 2002), the Nusselt  
910 number may be expressed as follows according to the convection regime:

911 Free convection:

$$912 \quad Nu = 0.59 (Pr_t \cdot Gr)^{0.25} \quad (A.3)$$

913 Mixed convection:

$$914 \quad Nu = 0.68 (Re^{1.5} + Pr_t^{0.75})^{0.33} \quad (A.4)$$

915



916 Forced convection:

$$917 \quad Nu = 0.67 Re^{0.5} Prt^{0.33} \quad (A.5)$$

918 where  $Re$  is Reynolds number;  $Gr$  is Grashof number and  $Prt$  Prandtl number equal to  
919 0.71 for air.

920 In the case of a greenhouse without mechanical ventilation, generally free convection  
921 prevails inside the greenhouse, and it follows that:

$$922 \quad r_a = \frac{\rho C_p d}{0.59 (Pr.Gr)^{0.25} \lambda_a} \quad (A.6)$$

## 923 **A.2 Leaf stomatal resistance**

924 The leaf stomatal resistance tunes the water vapour transfers through the leaf stomata (Fig.  
925 3), the opening stomata driving the transfer of water vapour between the inside of the leaf  
926 (where water vapour is saturating) and the surrounding air at leaf surface. They, thus,  
927 provide an additional resistance in serial with aerodynamic resistance.

928 Jarvis (1976) has proposed a multiplicative model of stomatal resistance integrating the  
929 influence of the different climatic variables on  $r_s$  (global radiation  $R_g$ , air vapor pressure  
930 deficit  $VPD_a$ , leaf temperature  $T_l$ , concentration of  $CO_2$  in the air  $C_a$ ). He also assumed that  
931 each variable acts independently.

$$932 \quad r_s = r_{smin} f_1(R_g) \cdot f_2(VPD_a) \cdot f_3(T_l) \cdot f_4(C_a) \quad (A.7)$$

933 where the  $f_i$  are empirical functions of the different variables studied. He also proposed  
934 empirical functions that take the following forms:  $f_1(R_g)$  is an asymptotic function (Table  
935 A1),  $f_2(VPD_a)$  a linear function,  $f_3(T_l)$  a hyperbolic function of the leaf temperature  $T_l$ ,  
936  $f_4(C_a)$  a partially linear decreasing function of the  $CO_2$  concentration  $C_a$ .

937 Further improvements on Jarvis' model have been proposed by other researchers such as  
938 Baille et al. (1994) to model the stomatal resistance of *Impatiens* who considered that for

939 the case of well-watered plants, the variables that most influence the functioning of the  
 940 stomata are the incident global radiation ( $R_g$ ) and air-air vapor pressure deficit  $VPD_a$ .

941

942 **Table A1.** The asymptotic function  $f_1(R_g)$  for different crops

Formula	Crop	Author
$f_1(R_g) = 1 + \left[ \exp(a_1 \cdot (R_g - b_1)) \right]^{-1}$	tobacco	Avissar et al, 1985
	tomato	Boulard et al., 1991
	banana	Demrati, 2007
$f_1(R_g) = 1 + \frac{a_1}{(R_g - b_1) \cdot c_1}$	tomato	Stanghellini, 1987
$f_1(R_g) = \frac{1 + a_1 \cdot R_g}{1 + b_1 \cdot R_g}$	not given	Farquhard, 1978
$f_1(R_g) = \frac{a_1 + R_g}{b_1 + R_g}$	9 ornamental species	Baille, 1994

943

944 where  $a_1$ ,  $b_1$  are parameters determined empirically from data collected in agricultural  
 945 greenhouse.

946 For  $VPD_a$ , Baille et al. (1994) established the following mathematical expression:

947 
$$f_2(VPD_a) = 1 + a_2(VPD_a - VPD_0)^2 \quad (A.8)$$

948 where  $VPD_0$  is the pressure deficit for which  $r_s$  is minimal.

949 For tomatoes another form has been proposed by Boulard et al. (1991) for  $VPD_a$  and  $T_a$ :

950 
$$f_2(VPD_a) = 1 + a_2 \exp(b_2(VPD_a - VPD_0)) \quad (A.9)$$

951 
$$f_2(T_a) = 1 + a_3 \exp(b_3(T_a - T_{max})) \quad (A.10)$$

952 where  $a_2$ ,  $a_3$  and  $b_2$ ,  $b_3$ ,  $VPD_0$  and  $T_{max}$  are also empirically determined parameters.

953 Other authors: Van Bavel (1978); Bot (1983) ; Kimball (1986); Stanghellini (1987); Jolliet  
954 et Bailey (1994), have also proposed relationships giving the stomatal resistance as a  
955 function of solar radiation and water vapor pressure.

956 In the case of water restriction, the water state of the soil or the plant becomes a limiting  
957 factor for closing or opening of the stomata. Nikolov et al. (1995) and Gang et al. (2012)  
958 add a stress function depending on the water potential of the soil and leaf:

959 
$$r_s = r_{smin} f_1(R_g) f_2(VPD_a) f_5(\Psi_s) \quad (A.11)$$

960

961 or 
$$r_s = r_{smin} f_1(R_g) f_2(VPD_a) f_5(\Psi_l) \quad (A.12)$$

962

963 **References**

- 964 Acock, B., Charles-Edwards, D. A., Fitter, D. J., Hand, D. W., Ludwig, L. J., Warren-  
965 Wilson, J. & Withers, A. C. (1978). The contribution of leaves from different levels  
966 within a tomato crop to canopy net photosynthesis: An experimental examination of  
967 two canopy models. *Journal of Experimental Botany*, 29, 815-27.
- 968 An C.H., Ri H. J., HanT.U., Kim S.I., Ju U.S. (2022). Feasibility of winter cultivation of  
969 fruit vegetables in a solar greenhouse in temperate zone; experimental and numerical  
970 study. *Solar Energy*, 233, 18-30.
- 971 Ansys-Fluent. (2010). Fluent V. 12.1. User's guide.
- 972 Avissar, R., Avissar P., Mahrer Y., and Bravdo B. (1985). A model to simulate response of  
973 plant stomata to environmental conditions. *Agricultural and Forest Meteorology*, 64,  
974 127–148.
- 975 Baille, M., Baille, A., Delmon, D. (1994a). Microclimate and transpiration of greenhouse  
976 rose crops. *Agricultural and Forest Meteorology*, 71, 83–97. doi:10.1016/0168-  
977 1923(94)90101-5
- 978 Baille, M., Baille, A., Laury, J.C. (1994b). A simplified model for predicting  
979 evapotranspiration rate of 9 ornamental species vs climate factor and leaf area. *Sci.*  
980 *Hortic. Amsterdam* 59, 217-232.
- 981 Bartzanas, T., Boulard, T. and Kittas, C. (2002). Numerical simulation of airflow and  
982 temperature patterns in a greenhouse equipped with insect-proof screen. *Computers and*  
983 *Electronics in Agriculture*, 34: 207 - 221.
- 984 Bartzanas, T., Boulard, T., & Kittas, C. (2004). Effect of Vent Arrangement on Windward  
985 Ventilation of a Tunnel Greenhouse. *Biosystems Engineering*, 88(4), 479- 490.  
986 <https://doi.org/10.1016/j.biosystemseng.2003.10.006>
- 987 Baxevanou, C., Fidaros, D., Katsoulas, N., Mekeridis, E., Varlamis, C., Zachariadis, A., &  
988 Logothetidis, S. (2020). Simulation of Radiation and Crop Activity in a Greenhouse  
989 Covered with Semitransparent Organic Photovoltaics. *Applied Sciences*, 10(7), 2550.  
990 <https://doi.org/10.3390/app10072550>
- 991 Ben Amara, H., Bouadila, S., Fatnassi, H., Müslüm A., Guizani A. A. (2021). Climate  
992 assessment of greenhouse equipped with south-oriented PV roofs: An experimental and  
993 computational fluid dynamics study. *Sustainable Energy Technologies and*  
994 *Assessments*, 45, 2021, 101100, ISSN 2213-1388,  
995 <https://doi.org/10.1016/j.seta.2021.101100>.
- 996 Bell, B. (2003). Application Brief: Film Condensation of Water Vapor. Lebanon, New  
997 Hampshire, USA: Fluent, Inc.

- 998 Bird, R.B., W.E. Stewart, and Lightfoot, E.N. (1960). *Transport Phenomena*, New York:  
999 John Wiley & Sons.
- 1000 Bot, G.P.A. 1983. Greenhouse climate: from physical processes to dynamic model. *Ph.*  
1001 *D. Thesis, Agricultural University, Wageningen, 240 pp.*
- 1002 Bouhoun Ali, H., Bournet, P.E., Danjou, V., Morille, B., Migeon, C. (2014). CFD  
1003 simulations of the night-time condensation inside a closed glasshouse: Sensitivity  
1004 analysis to outside external conditions, heating and glass properties. *Biosystems*  
1005 *Engineering*, 127, 2014, 159-175,  
1006 <https://doi.org/10.1016/j.biosystemseng.2014.08.017>.
- 1007 Bouhoun Ali, H., Bournet, P.E., Cannavo, P., & Chantoiseau, E. (2017). Development of a  
1008 CFD crop submodel for simulating microclimate and transpiration of ornamental plants  
1009 grown in a greenhouse under water restriction. *Computers and Electronics in*  
1010 *Agriculture*, <https://doi.org/10.1016/j.compag.2017.06.021>
- 1011 Bouhoun Ali, H., Bournet, P.-E., Cannavo, P., & Chantoiseau, E. (2018). Development of  
1012 a CFD crop submodel for simulating microclimate and transpiration of ornamental  
1013 plants grown in a greenhouse under water restriction. *Computers and Electronics in*  
1014 *Agriculture*, 149, 26- 40. <https://doi.org/10.1016/j.compag.2017.06.021>
- 1015 Bouhoun Ali, H., Bournet, P.-E., Cannavo, P., & Chantoiseau, E. (2019). Using CFD to  
1016 improve the irrigation strategy for growing ornamental plants inside a greenhouse.  
1017 *Biosystems Engineering*, 186, 130–145. [doi.org/10.1016/j.biosystemseng.2019.06.021](https://doi.org/10.1016/j.biosystemseng.2019.06.021)
- 1018 Boulard, T., Kittas, C., Roy J.C., Wang, S. (2002). Convective and ventilation transfers in  
1019 greenhouses, Part 2: Determination of the distributed climate. *Biosystem Engineering*  
1020 83 (2), 129-147.
- 1021 Boulard T., Roy, J.C., Fatnassi, H., Kichah, A., Lee, I-B. (2010). Computer Fluid Dynamics  
1022 prediction of climate and fungal spore transfer in a rose greenhouse. *Computers and*  
1023 *Electronics in Agriculture*, 74, 280-292.
- 1024 Boulard, T., Baille, A., Mermier, M., Vilette, F. (1991). Mesures et modélisation de la  
1025 résistance stomatique foliaire et de la transpiration d'un couvert de tomate de serre.  
1026 *Agronomie*, 11, 259-274.
- 1027 Boulard, T., Mermier, M., Fargues, J., Smits, N., Rougier, M., Roy, J.C. (2002). Tomato  
1028 leaf boundary layer climate: implications for microbiological whitefly control in  
1029 greenhouses. *Agricultural and Forest Meteorology*, 110, 159–176. [doi:10.1016/S0168-](https://doi.org/10.1016/S0168-1923(01)00292-1)  
1030 [1923\(01\)00292-1](https://doi.org/10.1016/S0168-1923(01)00292-1)

- 1031 Boulard, T., Roy, J.C., Pouillard, J.B., Fatnassi, H., Grisey, A. (2017). Modelling of  
1032 micrometeorology, canopy transpiration and photosynthesis in a closed greenhouse  
1033 using computational fluid dynamics. *Biosystems Engineering*, 158: 110 – 133.
- 1034 Boulard, T., Wang, S. (2002). Experimental and numerical studies on the heterogeneity of  
1035 crop transpiration in a plastic tunnel. *Computers and Electronics in Agriculture*, 34,  
1036 173–190. doi:10.1016/S0168-1699(01)00186-7.
- 1037 Bournet, P.E., Morille, B., Migeon, C. (2017). CFD prediction of the daytime climate  
1038 evolution inside a greenhouse taking account of the crop interaction, sun path and  
1039 ground conduction. *Acta Horticulturae*, 1170, 61–70.  
1040 <https://doi.org/10.17660/ActaHortic.2017.1170.6>.
- 1041 Brown, K.W., and W. Covey. (1966). The energy-budget evaluation of the micro-  
1042 meteorological transfer processes within a cornfield. *Agricultural Meteorology*, 3:73–  
1043 96.
- 1044 Bruse, M. (1995). Development of a micro-scale model for the calculation of surface  
1045 temperature in structured terrain. MSc thesis. Bochum, Germany: University of  
1046 Bochum, Institute for Geography.
- 1047 Cannavo, P., Bouhoun Ali, H., Chantoiseau, E., Migeon, C., Charpentier, S., Bournet, P.E.  
1048 (2016). Stomatal resistance of New Guinea Impatiens pot plants. Part 2: Model  
1049 extension for water restriction and application to irrigation scheduling. *Biosystems  
1050 Engineering*, 149, 82-93, doi:10.1016/j.biosystemseng.2016.07.001.
- 1051 CFD2000 manual (v3.0). (1997). Computational fluid dynamics systems. Pacific Sierra  
1052 Research Corporation, USA.
- 1053 Chen, J., Xu, F., Tan, D., Shen, Z., Zhang, L., Ai, Q. (2015). A control method for  
1054 agricultural greenhouses heating based on computational fluid dynamics and energy  
1055 prediction model. *Applied Energy* 141, 106–118.  
1056 <https://doi.org/10.1016/j.apenergy.2014.12.026>
- 1057 Cheng, X., Li, D., Shao, L., & Ren, Z. (2021). A virtual sensor simulation system of a  
1058 flower greenhouse coupled with a new temperature microclimate model using three-  
1059 dimensional CFD. *Computers and Electronics in Agriculture*, 181, 105934.  
1060 doi:10.1016/j.compag.2020.105934
- 1061 Defraeye, T., Derome D., Verboven P., Carmeliet J., Nicolai B. (2014). Cross-scale  
1062 modelling of transpiration from stomata via the leaf boundary layer. *Annals of Botany*,  
1063 114(4):711-23, doi:10.1093/aob/mct313.

- 1064 Demrati, H., Boulard, T., Fatnassi, H., Bekkaoui, A., Majdoubi, H., Elattir, H., Bouirden,  
1065 L. (2007). Microclimate and transpiration of a greenhouse banana crop. *Biosystems*  
1066 *Engineering*, 98, 66-78.
- 1067 Farquhar, G. D. (1978). Feedforward responses of stomata to humidity. *Australian Journal*  
1068 *of Plant Physiology*, 5, 787– 800.
- 1069 Fatnassi, H., Boulard, T., & Bouirden, L. (2003). Simulation of climatic conditions in full-  
1070 scale greenhouse fitted with insect-proof screens. *Agricultural and Forest Meteorology*,  
1071 118(1- 2), 97- 111. [https://doi.org/10.1016/S0168-1923\(03\)00071-6](https://doi.org/10.1016/S0168-1923(03)00071-6)
- 1072 Fatnassi, H., Boulard, T., Benamara H., Roy, J.C., Suay, R., Poncet, C. (2016). Increasing  
1073 the height and multiplying the number of spans of greenhouse: How far can we go?  
1074 *Acta Horticulturae*, 1170, 137-144, <https://doi.org/10.17660/ActaHortic.2017.1170.15>
- 1075 Fatnassi, H., Boulard, T., Poncet, C., & Chave, M. (2006). Optimisation of Greenhouse  
1076 Insect Screening with Computational Fluid Dynamics. *Biosystems Engineering*, 93(3),  
1077 301 - 312. <https://doi.org/10.1016/j.biosystemseng.2005.11.014>
- 1078 Fatnassi, H., Poncet, C., Bazzano, M. M., Brun, R., Bertin, N. (2015). A numerical  
1079 simulation of the photovoltaic greenhouse microclimate. *Solar Energy*, 120, 575- 584.  
1080 <https://doi.org/10.1016/j.solener.2015.07.019>
- 1081 Fidaros, D. K., Baxevanou, C. A., Bartzanas, T., & Kittas, C. (2010). Numerical simulation  
1082 of thermal behavior of a ventilated arc greenhouse during a solar day. *Renewable*  
1083 *Energy*, 35(7), 1380- 1386. <https://doi.org/10.1016/j.renene.2009.11.013>
- 1084 Gang, L., Yongyi, D., Dongsheng, A., Yongxiu, L., Weihong, L., Xinyou, Y., Chunjiang,  
1085 Z. (2012). Testing two models for the estimation of leaf stomatal conductance in four  
1086 greenhouse crops cucumber, chrysanthemum, tulip and liliun. *Agricultural and Forest*  
1087 *Meteorology*, 165, 92–103.
- 1088 Garzoli, K. V. (1985). A simple greenhouse climate model. *Acta Horticulturae*, 174, 393-  
1089 400.
- 1090 Goudriaan, J. (1977), *Crop Micrometeorology: A Simulation Study*, 1st ed., 249 pp., Centre  
1091 for Agricultural Publishing and Documentation, Wageningen, Netherlands
- 1092 Green, S. (1992). Modelling turbulent air flow in a stand of widely spaced trees. *Phoenics*  
1093 *Journal*, 5(3), 294–312.
- 1094 Guyot, G. (1999). In Dunod (Ed.). *Climatologie de l'environnement : cours et exercices*  
1095 *corrigés* (p. 525).

- 1096 Hang, X., Wang, H., Zou, Z., Wang, S. (2016). CFD and weighted entropy based simulation  
1097 and optimisation of Chinese Solar Greenhouse temperature distribution, *Biosystems*  
1098 *Engineering*, 142, 12-26, <https://doi.org/10.1016/j.biosystemseng.2015.11.006>.
- 1099 Haxaire, R. (1999). Caractérisation et Modélisation des écoulements d'air dans une serre.  
1100 Thèse de Docteur en Sciences de l'Ingénieur de l'Université de Nice, Sophia Antipolis.  
1101 148p.
- 1102 Jarvis (1976) The interpretation of the variations in leaf water potential and stomatal  
1103 conductance found in canopies in the field. *Phil. Trans. R. Soc. Lond. B* 273593–610.  
1104 <http://doi.org/10.1098/rstb.1976.0035>
- 1105 Jiao, W., Liu, Q., Lijun, G., Liu, K., Shi, R., Ta, N. (2020). Computational Fluid Dynamics-  
1106 Based Simulation of Crop Canopy Temperature and Humidity in Double-Film Solar  
1107 Greenhouse. *Hindawi Journal of Sensors*, Article ID 8874468, 15 pages  
1108 <https://doi.org/10.1155/2020/8874468>
- 1109 Jolliet, O., & Bailey, B. J. (1994). Hortitrans, a model for predicting and optimizing  
1110 transpiration and humidity in greenhouses. *Journal of Agricultural Engineering*  
1111 *Research*, 57, 23-37
- 1112 Katsoulas, N., Stanghellini, C. (2019). Modelling Crop Transpiration in Greenhouses:  
1113 Different Models for Different Applications. *Agronomy* 9(7):392.
- 1114 Kichah, A., Bournet, P.-E., Migeon, C., & Boulard, T. (2012). Measurement and CFD  
1115 simulation of microclimate characteristics and transpiration of an Impatiens pot plant  
1116 crop in a greenhouse. *Biosystems Engineering*, 112(1), 22- 34.  
1117 <https://doi.org/10.1016/j.biosystemseng.2012.01.012>
- 1118 Kim, R., Kim, J., Lee, I., Yeo, U., Lee, S., Decano-Valentin, C. (2021a). Development of  
1119 three-dimensional visualisation technology of the aerodynamic environment in a  
1120 greenhouse using CFD and VR technology, part 1 : Development of VR a database  
1121 using CFD. *Biosystems Engineering*, 207, 33- 58.  
1122 <https://doi.org/10.1016/j.biosystemseng.2021.02.017>
- 1123 Kim, R., Kim, J., Lee, I., Yeo, U., Lee, S., Decano-Valentin, C. (2021b). Development of  
1124 three-dimensional visualisation technology of the aerodynamic environment in a  
1125 greenhouse using CFD and VR technology, Part 2 : Development of an educational VR  
1126 simulator. *Biosystems Engineering*, 207, 12- 32.  
1127 <https://doi.org/10.1016/j.biosystemseng.2021.02.018>
- 1128 Kimball, B. A., (1986). A modular energy balance program including subroutines for  
1129 greenhouses and the other latent devices. U.S.D.A, Agricultural Research Service,  
1130 ARS-33, 360 pp



- 1131 Lee, I.B.; Yun, N.K.; Boulard, T.; Roy, J.C.; Lee, S.H.; Kim, G.W.; Lee, S.; Kwon, S.H.  
 1132 (2006). Development of an aerodynamic simulation for studying microclimate of plant  
 1133 canopy in greenhouse-(1) Study on aerodynamic resistance of tomato canopy through  
 1134 wind tunnel experiment. *Journal Bio-Environmental Control*, 15, 289–295.
- 1135 Lhomme, J.P., Katerji, N. (1991). A simple modelling of crop water balance for  
 1136 agrometeorological application. *Ecological Modelling*, 57, 11–25
- 1137 Liu R., Liu J., Liu H, Yang X., Bienvenido Barcena J.F., Li M. (2021). 3-D simulation of  
 1138 leaf condensation on cucumber canopy in a solar greenhouse. *Biosystems Engineering*  
 1139 210 (2021) 310 -329.
- 1140 Liu X, Li H, Li Y, Yue X, Tian S. (2020). Effect of internal surface structure of the north  
 1141 wall on Chinese solar greenhouse thermal microclimate based on computational fluid  
 1142 dynamics. *PLOS ONE* 15(4): e0231316. <https://doi.org/10.1371/journal.pone.0231316>
- 1143 Majdoubi H., Boulard T., Fatnassi H. and Bouirden L. (2009). Airflow and microclimate  
 1144 patterns in a one-hectare Canary type greenhouse: An experimental and CFD assisted  
 1145 study. *Agricultural and Forest Meteorology* 149, 1050-1062. ISSN 0168-1923,  
 1146 <https://doi.org/10.1016/j.agrformet.2009.01.002>.
- 1147 Majdoubi, H., Boulard, T., Fatnassi, H., Senhaji, A., Elbahi, S., Demrati, H., Mouqallid,  
 1148 M., Bouirden, L. (2016). Canary Greenhouse CFD Nocturnal Climate Simulation. *Open*  
 1149 *J. Fluid Dyn.* 06, 88–100. <https://doi.org/10.4236/ojfd.2016.62008> .
- 1150 Manzoni, S., Katul, G., Fay, P. A., Porporato, A. (2011). Modelling the  
 1151 vegetation-atmosphere carbon dioxide and water vapour interactions along a controlled  
 1152 CO<sub>2</sub> gradient. *Ecological Modelling*, 222, 653-665.
- 1153 Mistriotis, A., Arcidiacono, C., Picuno, P., Bot, G.P.A., Scarascia-Mugnozza, G. (1997a).  
 1154 Computational analysis of ventilation in greenhouses at zero and low-wind speed.  
 1155 *Agricultural and Forest Meteorology* 88, 121–135.
- 1156 Mistriotis, A., Bot, G.P.A., Picuno, P., Scarascia-Mugnozza, G. (1997b). Analysis of the  
 1157 efficiency of greenhouse ventilation using computational fluid dynamics. *Journal of*  
 1158 *Agricultural Engineering Research* 85, 217–228.
- 1159 Mistriotis, A., De Jong, T., Wagemans, M.J.M., Bot, G.P.A. (1997c). Computational fluid  
 1160 dynamics CFD as a tool for the analysis of ventilation and indoor microclimate in  
 1161 agricultural buildings. *Netherlands Journal of Agricultural Science* 45, 81–96.
- 1162 Molina-Aiz F.D., Fatnassi H., Boulard T., Roy J.C., Valera D.L. (2010). Comparison of  
 1163 finite element and finite volume methods for simulation of natural ventilation in  
 1164 greenhouses. *Computers and Electronics in Agriculture* 72 (2010) 69–86.

- 1165 Molina-Aiz, F. D., Valera D. L., Alvarez A. J., and Madueno A. (2006). A wind tunnel  
1166 study of airflow through horticultural crops: Determination of the drag coefficient.  
1167 *Biosystems Engineering*, 93(4): 447-457.
- 1168 Molina-Aiz, F.D., Norton, T., López, A., Reyes-Rosas, A., Moreno, M.A., Marín, P.,  
1169 Espinoza, K. and Valera, D.L. (2017). Using Computational Fluid Dynamics to analyse  
1170 the CO<sub>2</sub> transfer in naturally ventilated greenhouses. *Acta Horticulturae*, 1182, 283-  
1171 292. DOI: 10.17660/ActaHortic.2017.1182.34
- 1172 Monteith, J., Unsworth, M. (2013). Principles of environmental physics: plants, animals,  
1173 and the atmosphere. Academic Press
- 1174 Morille, B., Migeon, C., Bournet, P.E. (2013). Is the Penman–Monteith model adapted to  
1175 predict crop transpiration under greenhouse conditions? Application to a New Guinea  
1176 Impatiens crop. *Scientia Horticulturae*, 152, 80–91. doi:10.1016/j.scienta.2013.01.010
- 1177 Nebbali, R., Roy, J.C., Boulard, T. (2012). Dynamic simulation of the distributed radiative  
1178 and convective climate within a cropped greenhouse. *Renewable Energy* 43, 111–129.  
1179 doi:10.1016/j.renene.2011.12.003
- 1180 Nicot, P., Baille A. (1996). Integrated control of Botrytis cinerea on greenhouse  
1181 tomatoes. Aerial plant surface microbiology, Plenum Press, 1996, 0-306-45382-7.
- 1182 Nikolov, N.T., Massman, W.J., Schoettle, A.W. (1995). Coupling biochemical and  
1183 biophysical processes at the leaf level: an equilibrium photosynthesis model for leaves  
1184 of C<sub>3</sub> plants. *Ecological Modelling* 80, 205–235. doi:10.1016/0304-3800(94)00072-P
- 1185 Norton, T., Sun, D, Grant, J. Fallon, R., Dodd, V. (2007). Applications of computational  
1186 fluid dynamics (CFD) in the modelling and design of ventilation systems in the  
1187 agricultural industry: A review. *Bioresource Technology*, 98, 2386–2414
- 1188 Okushima, L., Sase, S., Nara, M. (1989). A support system for natural ventilation design  
1189 of greenhouse based on computational aerodynamics. *Acta Horticulturae* 248, 129–  
1190 136.
- 1191 Piscia, D., Montero, J.I., Baeza, E., Bailey, B.J. (2012). A CFD greenhouse night-time  
1192 condensation model. *Biosystems Engineering*, 111(2), 141-154.
- 1193 Pouillard, J.B., Boulard, T., Fatnassi, H., Grisey, A., Roy, J.C., (2012). Preliminary  
1194 experimental and CFD results on airflow and microclimate patterns in a closed  
1195 greenhouse. *Acta Horticulturae*, 952, 191-198 DOI: 10.17660/ActaHortic.2012.952.23
- 1196 Reichrath S., Davies T.W. (2001). CFD modelling of the Internal Environment of  
1197 commercial multi-span venlo-type glasshouses. Paper number 014054, 2001 ASAE  
1198 *Annual Meeting*, doi: 10.13031/2013.4276

- 1199 Roy J.C., Boulard T. (2003). CFD predictions of natural ventilation and climate in a tunnel  
1200 type greenhouse using a transpiration active crop model. *Acta Horticulturae*, 691, 457-  
1201 464, <https://doi.org/10.17660/ActaHortic.2005.691.55>
- 1202 Roy J.C., Boulard, T. (2005). CFD prediction of the natural ventilation in a tunnel-type  
1203 greenhouse: influence of wind direction and sensibility to turbulence models. *Acta*  
1204 *Horticulturae*, 457–464. doi:10.17660/ActaHortic.2005.691.55
- 1205 Roy, J.C., Boulard, T., Kittas, C., Wang, S. (2002). PA—Precision Agriculture. *Biosyst.*  
1206 *Eng.* 83, 1–20. doi:10.1006/bioe.2002.0107
- 1207 Roy, J.C., Pouillard, J.B., Boulard, T., Fatnassi, H. and Grisey, A. (2014). Experimental  
1208 and CFD results on the CO<sub>2</sub> distribution in a semi closed greenhouse. *Acta*  
1209 *Horticulturae*, 1037, 993-1000 DOI: 10.17660/ActaHortic.2014.1037.131
- 1210 Roy, J.-C., Vidal, C., Fargues, J., Boulard, T. (2008). CFD based determination of  
1211 temperature and humidity at leaf surface. *Computers and Electronics in Agriculture*,  
1212 (61) 201-212
- 1213 Sase, S., Kacira, M., Boulard, T., Okushima, L. (2012). Wind tunnel measurement of  
1214 aerodynamic properties of a tomato canopy. *Transactions of the ASABE*, 55(5): 1921-  
1215 1927
- 1216 Stanghellini, C. (1987). Transpiration of greenhouse crops. An aid to climate management.  
1217 PhD Thesis, Agricultural University, Wageningen.
- 1218 Tadj, N., Nahal, M.A., Draoui, B. and Kittas, C. (2017). CFD simulation of heating  
1219 greenhouse using a perforated polyethylene ducts. *International Journal of Engineering*  
1220 *Systems Modelling and Simulation*, 9(1), 3–11.
- 1221 Tamimi, E. A., Kacira, M., Choi, C., An, L. (2013). Analysis of microclimate uniformity  
1222 in a naturally vented greenhouse with a high-pressure fogging system. *Transactions of*  
1223 *the ASABE*. 56(3):1241-1254. DOI: 10.13031/trans.56.9985
- 1224 Thom, A.S. (1971). Momentum absorption by vegetation. *Qrtly J. Royal Meteorol. Soc.*  
1225 97(414): 414-428.
- 1226 Thornley, J.H.M. (1976). *Mathematical models in plant physiology*. Academic press,  
1227 London
- 1228 Tong, G., Christopher, D.M., Li, B. (2009). Numerical modelling of temperature variations  
1229 in a Chinese solar greenhouse. *Computers and Electronics in Agriculture*, 68 (1), 129–  
1230 139

- 1231 Tong, G., Christopher, D.M., Zhang, G. (2018). New insights on span selection for Chinese  
1232 solar greenhouses using CFD analyses. *Computers and Electronics in Agriculture*,  
1233 Volume 149, 2018, Pages 3-15, <https://doi.org/10.1016/j.compag.2017.09.031>.
- 1234 Van Bavel, C. H. M., Lascano R., Wil-son. D.R. (1978). Water relations of fritted clay.  
1235 *SoilSci. Soc. Amer. J.* 42:657-659.
- 1236 Van Bavel, C. H. M., Takakura, T., Bot, G. P. A. (1985). Global comparison of the  
1237 greenhouse climate models. *Acta Horticulturae*, 174, 21-33.
- 1238 Wang, X.W., . Luo, J.Y., Li X.P. (2013). CFD Based Study of Heterogeneous Microclimate  
1239 in a Typical Chinese Greenhouse in Central China. *Journal of Integrative Agriculture*,  
1240 12(5), 914-923, [https://doi.org/10.1016/S2095-3119\(13\)60309-3](https://doi.org/10.1016/S2095-3119(13)60309-3).
- 1241 Wilson, J.D., (1985) Numerical studies of flow through a windbreak. *J Wind Eng Ind*  
1242 *Aerodyn* 21:119–154
- 1243 Wu X., Liu X., Yue X., Xu H., Li T., and Li Y. (2021). Effect of the ridge position ratio on  
1244 the thermal environment of the Chinese solar greenhouse *R. Soc. open*  
1245 *sci.*8201707201707. <http://doi.org/10.1098/rsos.201707>
- 1246 Yu, G., Zhang, S., Li, S., Zhang, M., Benli, H., Wang, Y. (2022). Numerical investigation  
1247 for effects of natural light and ventilation on 3D tomato body heat distribution in a  
1248 Venlo greenhouse. *Information Processing in Agriculture*,  
1249 <https://doi.org/10.1016/j.inpa.2022.05.006>.
- 1250

1251 **Conflict of interest**

1252 The authors declare that they have no known competing financial interests or personal  
1253 relationships that could have appeared to influence the work reported in this paper.

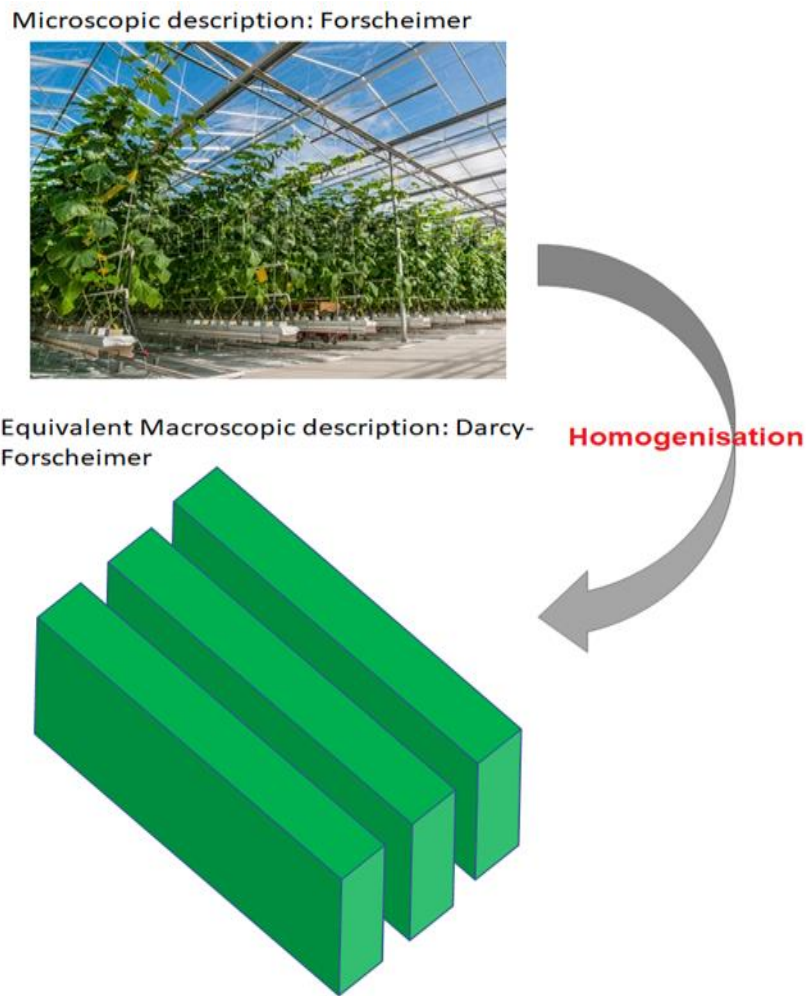


**Fig.1** Description of the crop: homogenization method

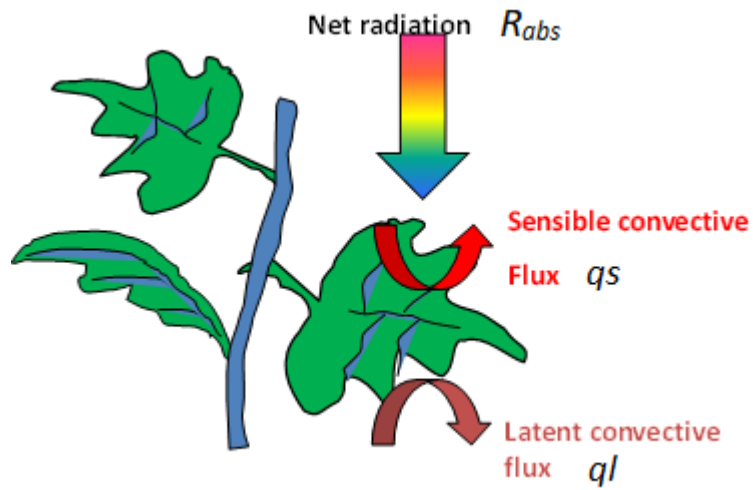


**Fig.2** Net radiation, sensible and latent heat balances of leaves

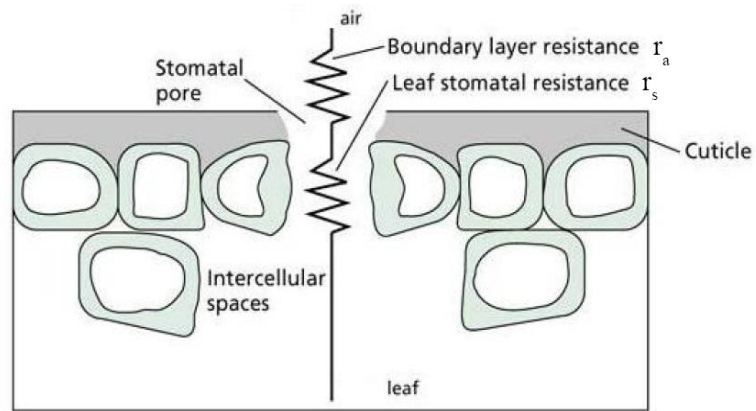


**Fig.3** Resistances to water vapor transfer between leaf and air



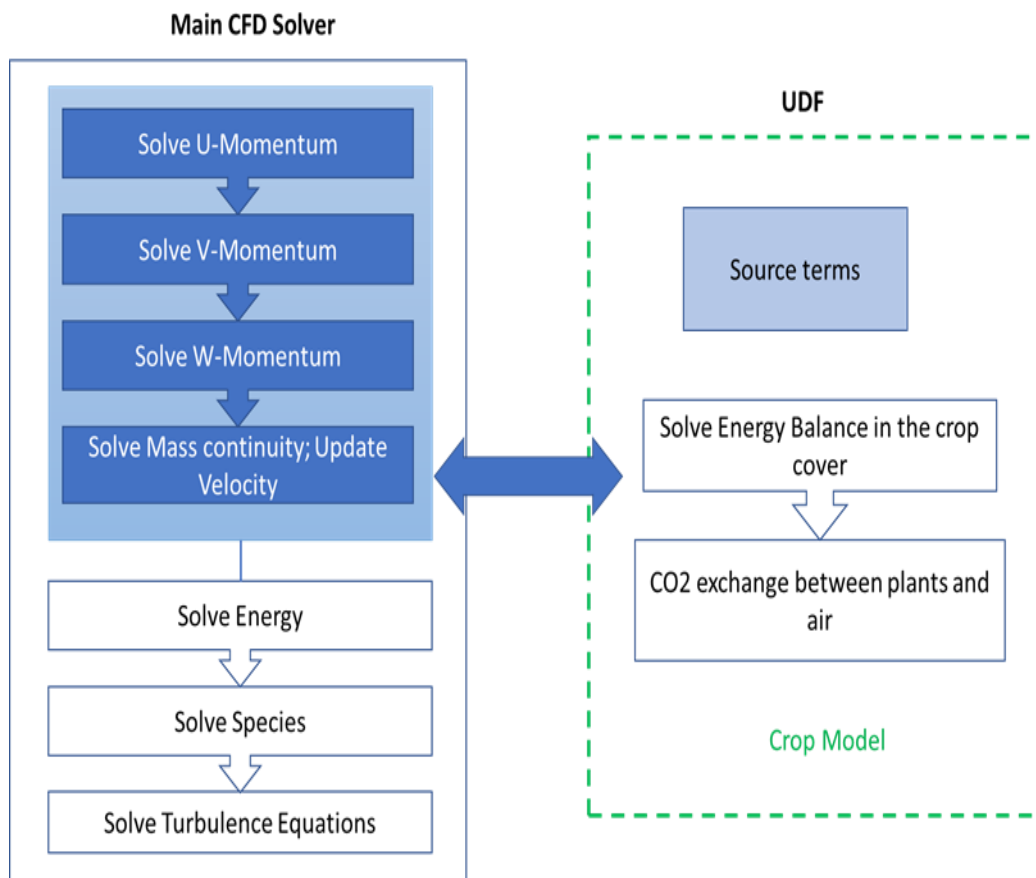


**Fig. 4** Sketch of the exchanges between the UDF and the main solver in the CFD model.

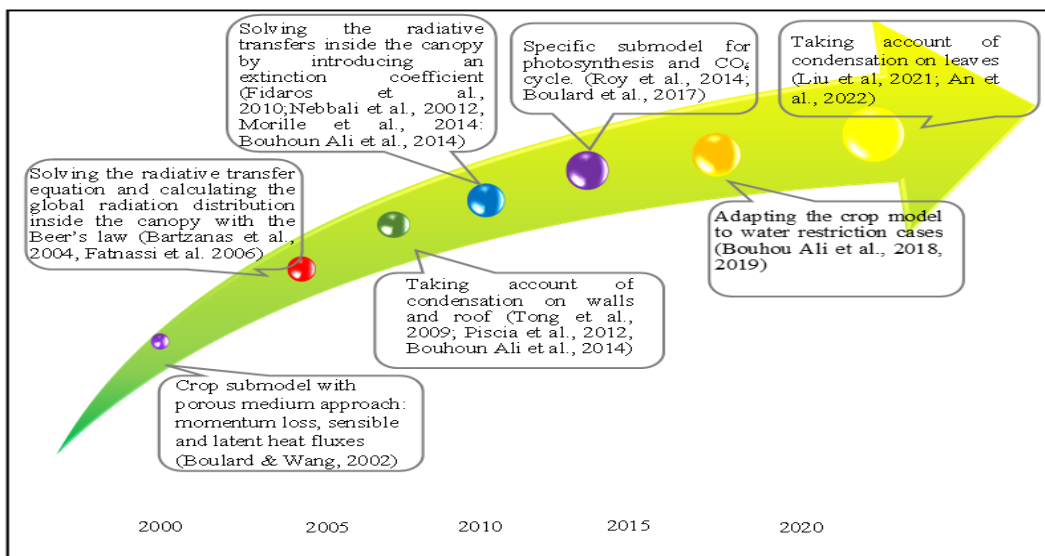


**Fig. 5** Milestones of CFD crop submodel developments

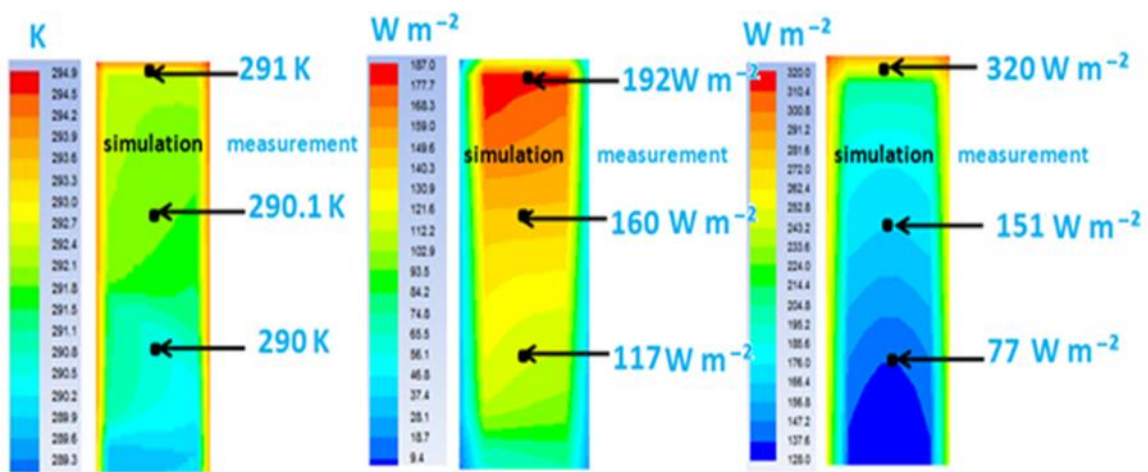


**Fig. 6** Simulated and measured distributions of leaf temperature in K (left), latent heat of crop transpiration in  $W m^{-2}$  (middle) and short wave radiations in  $W m^{-2}$  (right) within the crop cover at noon (after Pouillard et al., 2012).

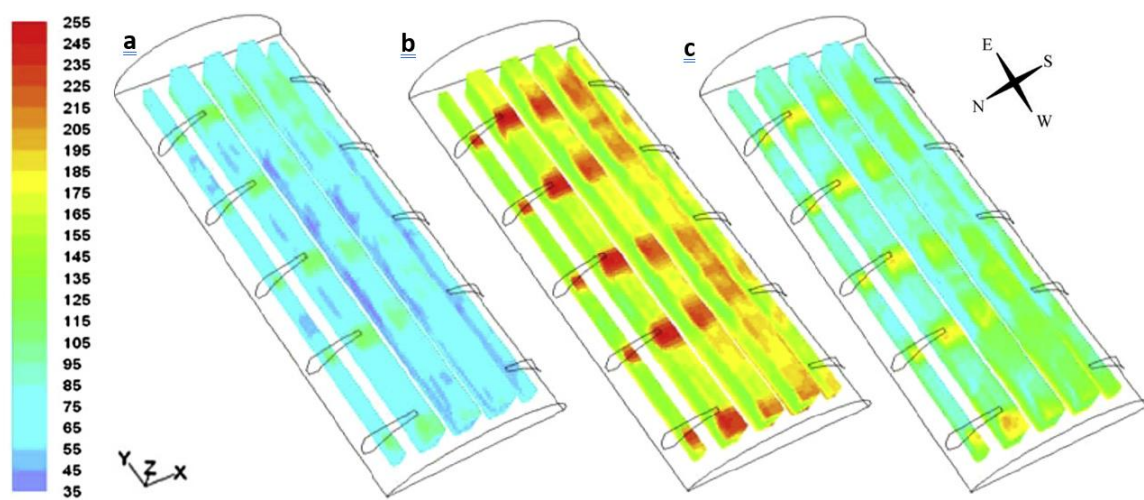


**Fig. 7** Distribution of the transpiration heat flux density on June 21<sup>st</sup>. (a): at sunrise, (b): at midday, (c): at sunset (after Nebbali et al., 2012)

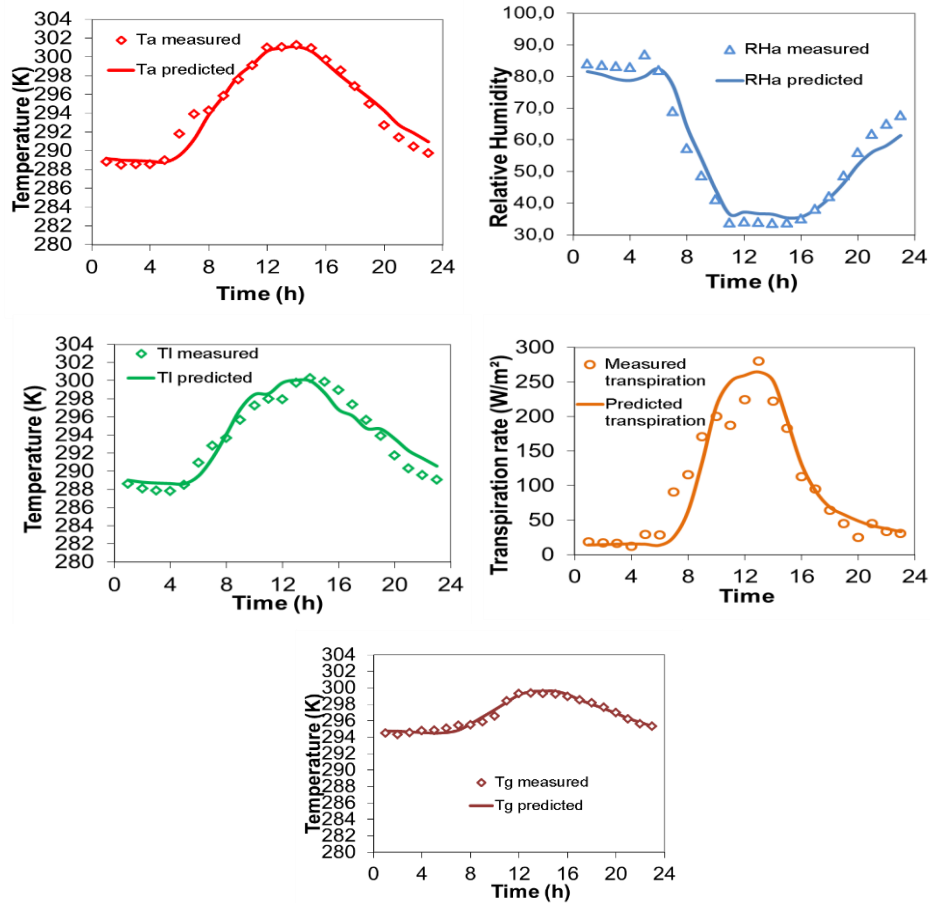


**Fig.8** Comparison of measurements and CFD simulations for A) air temperature above the crop; B) relative humidity above the crop; C) leaf temperature, D) transpiration rate and E) soil surface temperature (adapted from Bournet et al., 2017).

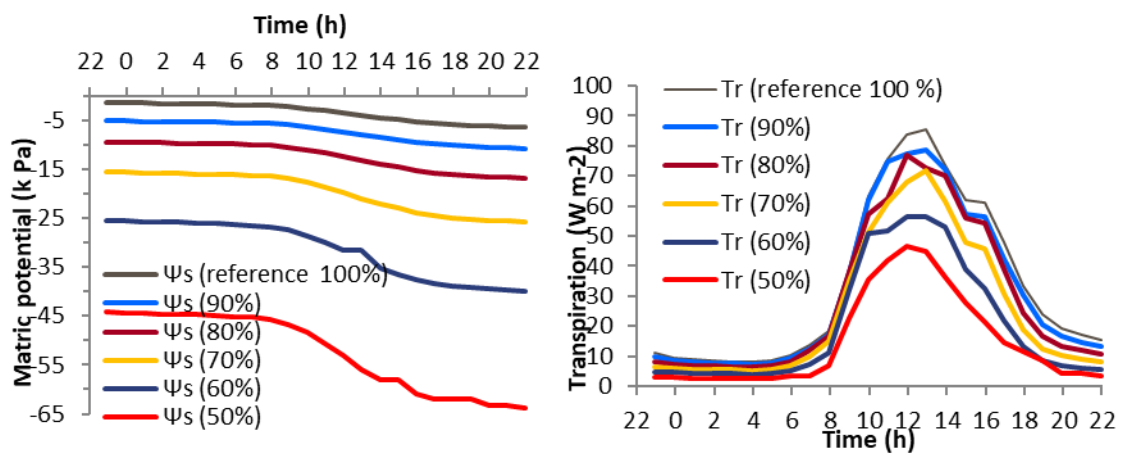


**Fig. 9** Evolution of the matric potential in the ground (a) and corresponding evolution of the evapotranspiration predicted by a CFD model for an impatiens crop (b) (after Bouhoun Ali et al., 2018)

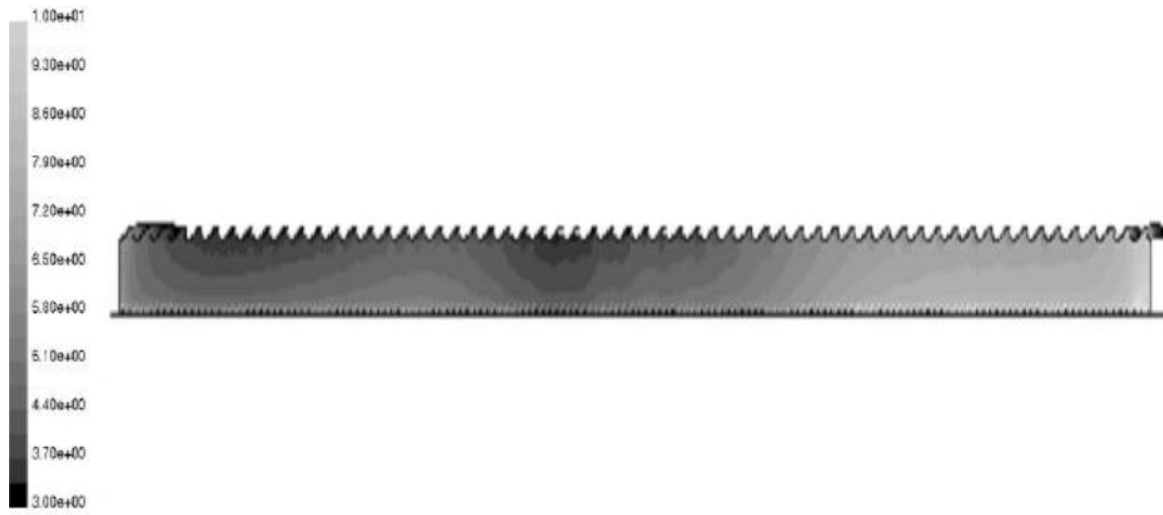


**Fig.10** Carbon dioxide dispersion in a 60 span Venlo-type glasshouse with crops (after Reichrath et al., 2001).

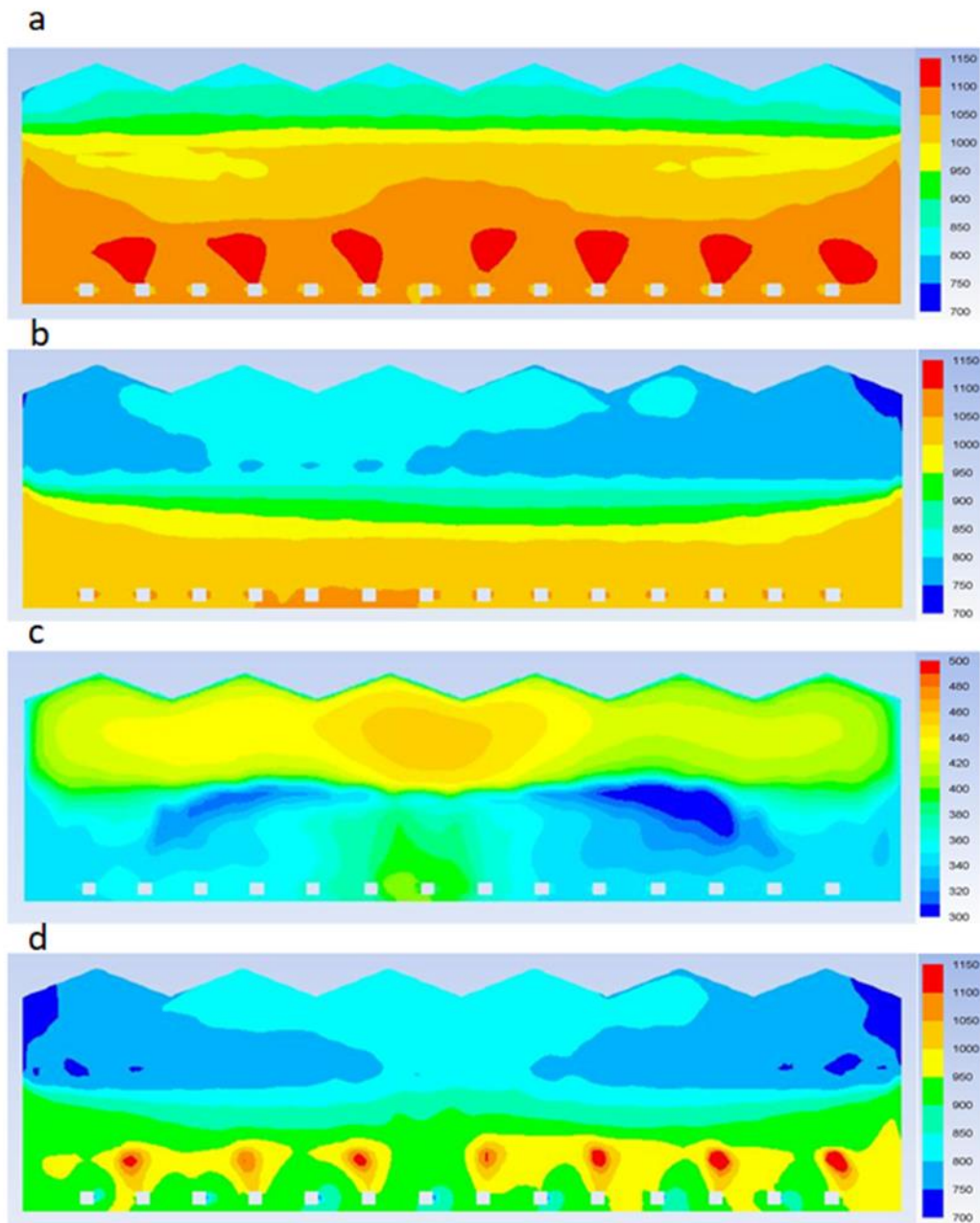


**Fig. 11.** Simulated carbon dioxide levels (ppm) in a median vertical transverse plane of the greenhouse at (a) 8:00 am; (b) 11:30 am; (c) 1:00 pm; (d) 5:30 pm. (After Boulard et al., 2017).



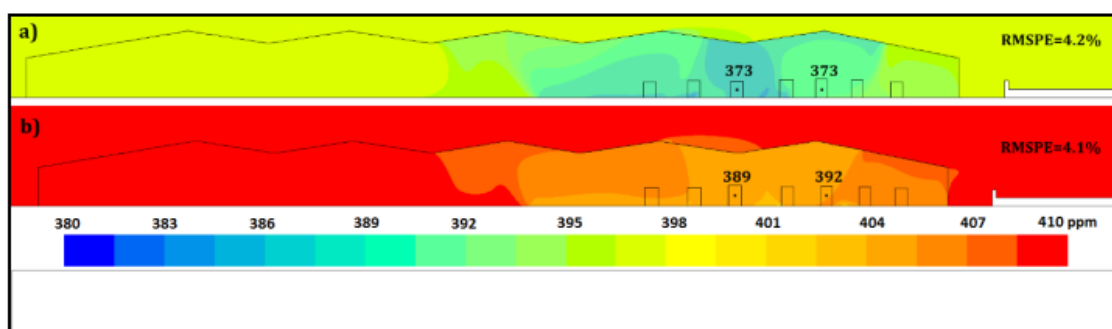


**Fig. 12.** Distributions of CO<sub>2</sub> concentration simulated with CFD and measured values (indicated in the figures) in the greenhouse on (a) 3/11/2014 and (b) 3/13/2014. (After Molina et al., 2017)

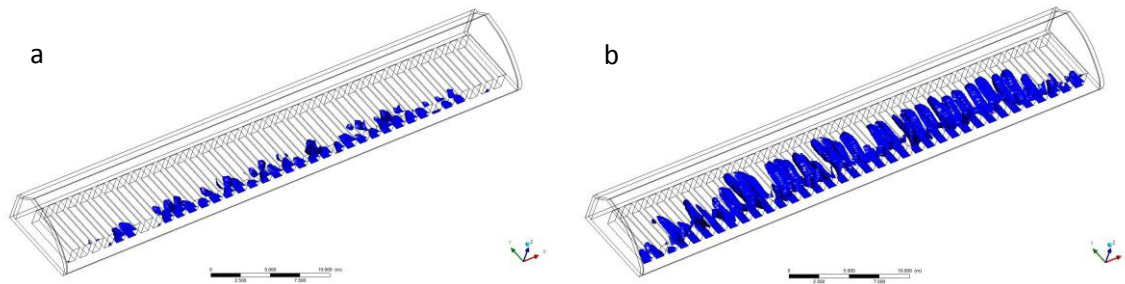


**Fig. 13.** Simulated leaf condensation on April 17 at (a) 01:30 and (b) 05:30. Y represents the north; X represents the east; and ■ represents the condensation that appeared based on simulation (after Liu et al., 2021).

**Table 1.** Validation studies of the CFD model based on the comparison between measured and simulated values of climate parameters in the greenhouse

<b>Authors</b>	<b>Greenhouse type</b>	<b>Crop</b>	<b>Dimension</b>	<b>Validation</b>
Boulard & Wang (2002)	Tunnel	Lettuce	3D steady	Transmittance, air velocity Temperature, transpiration flux
Fatnassi et al. (2003)	Moroccan type	Tomato	3D steady	Ventilation rate
Bartzanas et al. (2004)	Tunnel	Tomato	2D/3D steady	Air velocity, ventilation rate, air temperature
Fatnassi et al. (2006)	Multi span	Roses	3D steady	Ventilation rate
Majdoubi et al. (2009)	Canary type	Tomato	3D steady	Air temperature, relative humidity
Tong et al. (2009)	Chinese	Lettuce	2D unsteady	Air temperature
Boulard et al. (2010)	Multispan plastic	Roses	2D unsteady	Air temperature and humidity, spore concentration
Piscia et al. (2012a)	4-span plastic	Lettuce	3D unsteady	Air temperature, roof temperature, humidity ratio
Tamimi et al. (2013)	Arch type	Tomato	3D steady	Air velocity, evapotranspiration, stomatal resistance
Majdoubi et al. (2016)	Canarian	Tomato	3D steady	Air temperature and humidity
Bouhoun Ali et al. (2018)	Venlo glass house	New Guinea Impatiens	2D unsteady	Air temperature, leaf temperature matric potential, stomatal resistance, air humidity, transpiration rate
Boulard et al. (2017)	6-span glasshouse	Tomato	3D unsteady	Air temperature, leaf temperature, saturated humidity at leaf temperature, air humidity, shortwave radiation, air speed, crop transpiration, CO <sub>2</sub> concentration
Bouhoun Ali et al. (2019)	Venlo glass house	New Guinea Impatiens	2D unsteady	Air temperature and humidity, stomatal resistance, ventilation rate
Fatnassi et al. (2021)	Four-span plastic arched greenhouse	Rose	3D unsteady	Air temperature and humidity

**Table A1.** The asymptotic function  $f_1(R_g)$  for different crops

Formula	Crop	Author
$f_1(R_g) = 1 + \left[ \exp \left( a_1 \cdot (R_g - b_1) \right) \right]^{-1}$	tobacco	Avissar et al, 1985
	tomato	Boulard et al., 1991
	banana	Demrati, 2007
$f_1(R_g) = 1 + \frac{a_1}{(R_g - b_1) \cdot c_1}$	tomato	Stanghellini, 1987
$f_1(R_g) = \frac{1 + a_1 \cdot R_g}{1 + b_1 \cdot R_g}$	not given	Farquhard, 1978
$f_1(R_g) = \frac{a_1 + R_g}{b_1 + R_g}$	9 ornamental species	Baille, 1994

Editorial Office  
Academic Editor  
Biosystems Engineering Journal

Dear Professor Nikolaos Katsoulas ,

Please find enclosed, the revised version of our manuscript “YBENG-D-22-01328”, for publication in Biosystems Engineering Journal, by Hicham Fatnassi et al. entitled “*Use of Computational Fluid Dynamic tools to model the coupling of plant canopy activity and climate in greenhouses and closed plant growth systems: a review*”.

I have carefully considered each comment and made the necessary changes to the text. As you will see from the margin notes, I have addressed all your concerns.

I would like to express my gratitude for the time and effort you and the reviewers have invested in reviewing my manuscript. The comments and suggestions have been invaluable in improving the quality of the manuscript, and I believe that the revised version represents a significant improvement over the original submission.

Sincerely yours,

Hicham Fatnassi and co-authors